System model derivation of the CO_2 two-phase ejector based on the CFD-based reduced-order model

Michal Haida[a,*], Jacek Smolka[a], Armin Hafner[b], Ziemowit Ostrowski[a], Michal Palacz[a], Andrzej J. Nowak[a], Krzysztof Banasiak[c]

[a]*Institute of Thermal Technology, Silesian University of Technology, Konarskiego 22, 44-100 Gliwice, Poland*
[b]*NTNU Department of Energy and Process Engineering, Kolbjørn Hejes vei 1d, 7465 Trondheim, Norway*
[c]*SINTEF Energy, Kolbjørn Hejes vei 1d, 7465 Trondheim, Norway*

Abstract

The developed reduced-order model (ROM) of the R744 two-phase ejector was presented in this paper. The proper orthogonal decomposition (POD) model was employed together with the radial basis function (RBF) to evaluate the ejector performance at the motive nozzle operating regime from 70 bar to 100 bar. The proposed model was built based on the full CFD model of the R744 two-phase ejector with homogeneous equilibrium flow assumption. The validation procedure was performed to evaluate the ejector nozzles mass flow rate discrepancies of ROM compared to the CFD results and experimental data. In addition, the accuracy analysis of the ROM flow field results compared to the CFD results was performed. The validation process based on the CFD results and experimental data indicated the high accuracy of ROM for both nozzles mass flow rate within ±10% for most of the investigated operating points. Hence, the high accuracy of the computed mass flow rates allows ROM implementation into the dynamic simulations of the refrigeration system to evaluate the ejector performance at given operating points with negligible time effort.

Keywords: carbon dioxide, refrigeration system, two-phase ejector, reduced-order model, ejector-based system, CFD modelling

1. Introduction

The recent restrictive legal regulations for environmental protection led to the design of modern comparative refrigeration systems that use natural refrigerants [1]. Carbon dioxide (denoted as R744) has been applied in vapour compression refrigeration for over 130 years, and it is classified as a non-toxic and non-flammable fluid with a low global warming potential index (GWP) of 1 and ozone depletion potential index of 0 [2]. However, the typical R744 direct expansion systems are characterised by relatively high thermodynamic losses in the high-pressure expansion valve, which is the primary motivation to search for system energy performance improvement [3]. Modern CO_2 refrigeration systems possess an additional liquid receiver to decrease the pressure ratio of the high-pressure expansion valve and the saturated flash gas from the receiver is either expanded to the medium-temperature evaporator pressure level or directly compressed to the high-pressure gas cooler pressure level by an additional compressor [4, 5]. However, there is still a considerable potential to improve the energy performance of such refrigeration systems. One of the solutions is the use of the two-phase ejector either as a main expansion device instead of the high-pressure expansion valve [6], or as a liquid ejector to recirculate the liquid refrigerant in the flooded evaporator [7].

*Tel.: +48 322372810; fax: +48 322372872
Michal.Haida@polsl.pl

The two-phase ejector is a device without moving parts that contains a converging-diverging inlet nozzle for high-pressure streams, a suction inlet for low-pressure streams, the mixing section and outlet diffuser [8]. The primary aim of the ejector operation is to expand the motive nozzle fluid, entrain the suction nozzle flow, and compress the mixed flow to the intermediate-pressure level. Therefore, the implementation of the well-designed two-phase ejector as an expansion device in the R744 refrigeration system recovered potential work and improved the system performance by the compression of the entrained medium-temperature refrigerant to the intermediate pressure-level without additional energy consumption [6].

An improvement of the R744 ejector-based refrigeration system over the standard direct expansion system or booster system was reported in many papers that were reviewed in [9]. The authors stated that the coefficient of performance (COP) improvement of the R744 transcritical ejector-based system was in the range of 6% to 55% for thermodynamic analyses and from 7% to 20% for experimental investigations. The CO_2 refrigeration systems with ejector-expansion devices were applied and installed in either cold climates, such as Scandinavia, or warm climates, such as Italy, for supermarket applications [10, 11].

The dynamic change of the operating conditions in the supermarket applications due to the annual demand of the air conditioning load, cooling load, and heat-pump load required the modification of the R744 ejector-based system to obtain high performance under different ejector capacity. Hence, the multi-ejector concept for CO_2 supermarket refrigeration systems was proposed by Hafner et al. [10]. The authors stated that the high-side pressure was able to be controlled by the non-continuously standard ejectors with different motive nozzle cross-sectional area relative to the ambient temperature and load requirements. The investigation was performed on the object-oriented dynamic simulations for three European cities located in different climate zones. Moreover, the climate annual data were taken from the external meteorological databases. According to Hafner et al. [10], the COP improvement of the R744 multi-ejector refrigeration system was obtained for nearly all operating conditions in each climate zone, especially for the Mediterranean region in the summer season up to 17%. Apart from the multi-ejector concept, integration of the adjustable ejector with the CO_2 refrigeration system let the system performance improve due to the highly efficient work of the ejector at various operating conditions and cooling capacity [12]. Liu et al. [12] stated that the improvement of the R744 air conditioning system equipped with the controllable ejector was 36% compared to the conventional system with the expansion valve.

The multi-ejector module concept was experimentally validated by Banasiak et al. [13]. The development and performance mapping of prototype parallel ejectors were performed for typical supermarket loads under different operating conditions. The four vapour ejectors with differentiated capacity in binary order were designed and integrated with the module to dynamically utilise the multi-ejector module with an optimal efficiency for different conditions. The authors stated that the system performance improvement for ejector efficiency was up to 30% together with the overall compressor efficiency approximately at the optimal value. According to Haida et al. [14], the experimental investigation of the R744 multi-ejector refrigeration system confirmed the maximum COP improvement of that system by up to 7% compared to the R744 refrigeration system with the parallel compression of the flash gas.

Apart from the supermarket applications, the R744 ejector-based vapour compression unit was investigated as a hybrid ejector CO_2 compression cooling system for vehicles [15]. The authors performed thermodynamic simulations based on the one-dimensional ejector model presented by Eames et al. [16]. In addition to the simulation performance, a preliminary experimental investigation was conducted. Chen et al. [15] concluded that the COP of the hybrid ejector CO_2 cooling system improved to approximately 45% compared to the single CO_2 vapour compression system and the discrepancies of COP given by the simulations were within ±15% when compared to the experimental data. Moreover, the COP improvement of the system equipped with the ejector was reported for supercritical CO_2 Brayton cycles in [17]. The proposed system equipped with the ejector-expansion device was compared to the conventional supercritical CO_2 Brayton cycle. The authors stated that the R744 ejector-based system was able to achieve higher thermal efficiency than the referenced steam Rankine cycles at certain operating conditions.

Each mentioned thermodynamic simulation was based on the mathematical component model used in this study to simplify the more complex phenomena of the energy efficiency evaluation for each refrigeration component. Therefore, the Kornhauser zero-dimensional homogeneous equilibrium model of the ejector was mostly used in the thermodynamic analysis [18]. The foregoing model assumed constant fluid properties, as well as mixing pressure below the evaporation pressure throughout the mixing section, negligible kinetic energy influence outside of the ejector, and constant nozzle and diffuser efficiencies to evaluate deviation from the adiabatic reversible processes. Elbel et al. [19] stated that for CO_2 two-phase ejector the assumed efficiencies were 0.8 for both nozzles and 0.75 for the diffuser in the R744 ejector-based refrigeration system simulations. The assumption of constant efficiency for ejector components is a principal drawback of the Kornhauser ejector model due to a strong dependency of the efficiency values on the operating conditions [20]. Liu and Groll [21] proposed empirical correlations of the nozzle efficiency and mixing sections to perform the simulations of the R744 ejector-based refrigeration system for different operating conditions and ejector geometry. The authors stated that the accuracy of predicted COP and the cooling capacity of the R744 ejector-based air-conditioning system for the various ejector geometries and operating conditions were within ±8% and ± 12%, respectively. Richter [22] proposed an object-oriented equation-based model of the ejector to perform the transient simulations of the refrigeration system. The author computed the mass flow rate through the nozzle by use of the Bernoulli equation for single-phase flow and the constant value of the effective area was assumed. The simulated ejector efficiency discrepancy was within ±30% compared to the experimental results of the prototype R744 ejector at transcritical operating conditions. Therefore, the more complex numerical model of the ejector should be implemented in the dynamic simulation model. The primary aim of the foregoing implementation was to ensure the ejector mapping for the dynamic change of the ambient temperature and the cooling demand with the high accuracy of the ejector model results.

The numerical approach enabled the evaluation of the ejector performance at proper operating conditions, although the implementation of each CFD model in the dynamic simulations is impossible due to the computation time for a single operating point. Hence, the idea of building a fast approximate model, that would replace the complex CFD model of the ejector, arises in a natural way. Such a reduced order, yet accurate, model would allow implementation in the dynamic system simulations, while keeping high accuracy in a wide range of operating conditions. One of the solutions is to use the reduced-order model (ROM) based on the proper orthogonal decomposition (POD) approximation basis. The most important advantage of such a choice for the approximation base is its optimality, i.e., there is no other approximation base with smaller error. Due to this property, the ROM constructed using the full CFD model of two-phase flow is characterised by very high accuracy, while the computational time is decreased significantly.

The investigation of the two-phase flow dynamics inside the converging-diverging nozzle using a robust POD method was performed by Danlos et al. [23]. In that work, the POD method was used to identify the cavitation regimes by the sequences of the sheet cavity images. Moreover, the authors concluded that POD enabled the investigation of the groove effects of the cavity. Brenner et al. [24] presented the implementation and the derivation of the POD-ROM for non-isothermal multiphase flow. The ROM was developed on the two-dimensional CFD model of the non-isothermal fluidised bed. The authors stated that the results given by the POD-ROM were identical to the CFD model results. To make the ROM a continuous function of the input parameters used to generate the snapshot and to minimise the number of numerical simulations, the radial basis function (RBF) interpolation method was implemented to the POD-ROM [25]. The RBF interpolation technique was successfully applied in many applications, e.g., in the multiphase flow investigations as an RBF neural network [26, 27]. The POD-RBF approach was used to solve the inverse heat transfer problems in [28] and as the approximation of radiative properties of the gas mixtures [29].

The implementation of the ejector ROM in the dynamic simulation of the R744 refrigeration system led to the analysis of the influence of the designed ejector on the system performance at various operating conditions and cooling capacity. To the best knowledge of the authors, an ROM has not been applied to the R744 refrigeration system so far. Therefore, the primary aim of the presented paper is to build a lower order, but accurate, model of the CO_2 two-phase ejector based on the complex CFD model of the two-phase ejector.

The numerical analysis of the R744 ejector led to the investigation of the local flow phenomena inside the two-phase ejector, which can be used to either evaluate the performance of the existing ejector or design the ejector under specified operating conditions [20]. The numerical model of the R744 ejector used to generate the proposed ROM is a three-dimensional CFD model of the R744 transcritical ejector with a homogeneous equilibrium flow assumption developed by Smolka et al. [30]. The authors implemented an enthalpy-based form and real fluid properties from the REFPROP libraries [31], as a substitution for the temperature-based energy equation for simulating carbon dioxide transonic flow inside the two-phase ejector. The accuracy of the foregoing homogenous equilibrium model (HEM) was investigated by Palacz et al. [32] for typical supermarket operating conditions. The acceptable accuracy of the HEM results for the R744 two-phase ejector was for near or above the critical point.

The CFD model of the two-phase ejector with the HEM assumption is presented in Section 2. The POD model was built based on the Karhunen-Loève transformation for mapping the transcritical and close to critical point operating regimes of the motive fluid for which the numerical model results obtained high mass flow rate accuracy [32]. The detailed description of the ROM approach can be found in Section 3. The validation of the truncated POD-RBF model was performed for numerical results and the experimental data of the investigated ejector. The validation procedure is described in Section 4 and the results followed by the discussion are in Section 5. The study's conclusions are presented in Section 6.

2. Numerical Model

The detailed description of the numerical model and the computational procedure is presented in this section. First, the mathematical formula of the HEM is described in Section 2.1. Moreover, the computational procedure of the numerical model as well as the ejector geometry, mesh quality, turbulence model and thermodynamic properties are presented in Section 2.2.

2.1. HEM approach

The main assumption of the HEM is the equilibrium state between the liquid phase and the vapour phase of the two-phase flow. Therefore, the local quantities of pressure, temperature and velocity are the same for both phases, and the thermal non-equilibrium effects are omitted. The homogeneous equilibrium flow assumption simplifies the numerical model to the mass, momentum and energy governing equations of the equilibrium mixture. In addition, steady-state computations were performed for each operating condition; therefore, all of the time derivatives in the governing equations were omitted. The mass balance is described as follows:

$$\nabla \cdot \left(\rho \mathbf{U}\right) = 0 \tag{1}$$

where ρ is the fluid density in kg/m^3, t is the time in second and $\mathbf{U}$ is the fluid velocity vector in m/s. The momentum balance is defined by the following equation:

$$\nabla \cdot \left(\rho \mathbf{U}\mathbf{U}\right) = -\nabla p + \nabla \cdot \tau \tag{2}$$

where p is the pressure of the mixture fluid in Pa and τ is the stress tensor in N/m^2. According to Smolka et al. [30], the temperature-based form of the energy equation can be replaced by the enthalpy-based form. Hence, the energy balance can be defined as follows:

$$\nabla \cdot \left(\rho \mathbf{U} E\right) = \nabla \cdot \left[\left(\frac{k}{\frac{\partial h}{\partial T}}\right)_p \nabla h - \left(\frac{k}{\frac{\partial h}{\partial T}}\right)_p \left(\frac{\partial h}{\partial p}\right)_T \nabla p + \tau \cdot \mathbf{U}\right] \tag{3}$$

where T is the mixture temperature in K, k is the thermal conductivity in $W/(m^2 \cdot K)$ and E is the total specific enthalpy defined as a sum of the specific mixture enthalpy and the kinetic energy:

$$E = h + \frac{U^2}{2} \tag{4}$$

where h is the mixture specific enthalpy in $J/(kg \cdot K)$. The enthalpy-based form of the energy equation and the homogeneous equilibrium model assumption allow one to define fluid properties as a function of the equilibrium mixture pressure and specific enthalpy:

$$\left\{\rho, \mu, k, c_p\right\} = f\left(p, h\right) \tag{5}$$

where μ is the dynamic viscosity in $Pa \cdot s$ and c_p is the specific heat in $J/(kg \cdot K)$. Finally, the mathematical model of the two-phase flow was defined and the HEM was implemented to the discretised domain of the R744 two-phase ejector to perform the numerical computations at specified operating conditions.

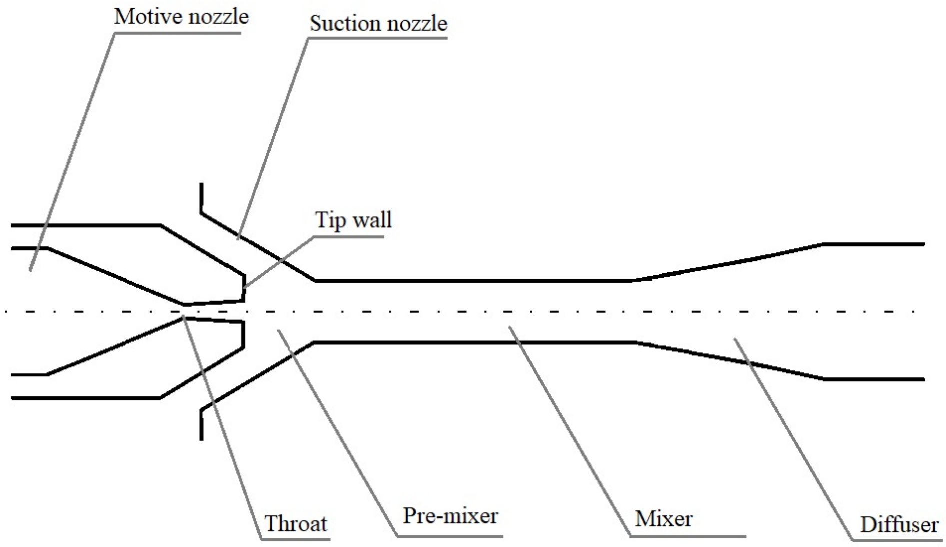

Figure 1: Geometry assembly of the R744 two-phase ejector.

2.2. Computational procedure

The CFD simulations of the R744 two-phase ejector were performed based on the HEM mathematical formulation in Ansys Fluent commercial software [30]. The *ejectorPL* platform was used to automate throughout the simulation process by generating the numerical grid in an Ansys ICEM CFD mesh generator, performing the numerical computations and processing the resulting data in the solver Ansys Fluent. Moreover, the *ejectorPL* controlled and combined geometric input data together with the mesh generation and the post-processing prepared to generate the ROM.

The R744 two-phase ejector geometric assembly together with the primary ejector components is shown in Fig. 1. It can be seen that the ejector consists of the converging-diverging motive nozzle, a converging suction nozzle, a pre-mixer with varying cross-section, a mixer with fixed cross-section and a diffuser. The designed fixed ejector was installed in the multi-ejector module that was experimentally validated and mapped by Banasiak et al. [13]. The multi-ejector module was equipped with four R744 vapour fixed ejectors of different ejector capacity changed in a binary order (1:2:4:8) to obtain high-efficiency expansion performance for different cooling demands and ambient conditions. The dimensions of the investigated ejector are presented in Table 1.

According to the ejector shape presented in Fig. 1, the numerical model was defined as the two-dimensional axisymmetric CFD model, which significantly reduced the size of the numerical grid. Hence, the mesh was generated by approximately 20,000 hexahedral elements. Moreover, the minimum orthogonal quality was 0.9, confirming the negligible influence of element shape on the results. The wall roughness was set to 2 μm according to the ejectors manufacturers [33]. The ejector mesh independence study was provided in the previous studies where the discretisation process was also presented [30, 34].

Apart from the generated mesh and the HEM mathematical model, the set of boundary conditions on the boundary mesh surfaces and the discretisation scheme are required to perform the numerical computations. Hence, the pressure and the temperature boundary values were selected for the motive and suction inlets and the pressure was selected for the ejector outlet. The set of the boundary conditions to perform the CFD simulation was described in Section 4.1. The partial differential equations of the mathematical model were solved based on the PRESTO scheme for pressure discretisation and the second-order upwind scheme for the other variables considered in the HEM. The coupled method was employed for the coupling of pressure and velocity.

The R744 two-phase flow behaviour was modelled using the realisable $K-\epsilon$ turbulence model. The foregoing two-equation turbulence model applied in the HEM for CO_2 two-phase ejector was tested by Smolka et al. [30]

Table 1: The main geometry parameters of the R744 two-phase ejector installed in the multi-ejector module [13].

Parameter name	Unit	Dimension
Motive nozzle inlet diameter	10^{-3} m	3.80
Motive nozzle throat diameter	10^{-3} m	1.00
Motive nozzle outlet diameter	10^{-3} m	1.12
Motive nozzle converging angle	°	30.00
Motive nozzle diverging angle	°	2.00
Diffuser outlet diameter	10^{-3} m	7.30
Diffuser angle	°	5.00

with succesful results. Moreover, this turbulence model was also used to define application range of HEM for R744 two-phase ejector in the work of Palacz et al. [32]. In that paper, the validation procedure was performed to define the mass flow rate discrepancies of both nozzles in the subcritical and transcritical regimes under the operating conditions typical for supermarket application. The satisfactory accuracy of ±10% for the motive nozzle and suction nozzle mass flow rates was obtained.

According to the HEM assumption and enthalpy-based energy equation, the real fluid properties were defined as a function of pressure and specific enthalpy. Therefore, the REFPROP libraries were implemented in the Fluent solver [31]. The use of the mentioned thermodynamic libraries allowed one to define the real fluid properties of the CO_2 flow in the two-phase region inside the ejector.

Finally, the solution of the prepared model converged when the mass imbalance of the inlet and outlet mass flow rates was very low, and each mass flow rate was stabilised in the boundary region. The entire computational time for a single operating point was approximately 30 minutes for the test case using two-node parallel processes. After the computation, contour plots and ejector performance data for both variables were exported. Moreover, the set of each variable for the whole domain was exported to the dataset file that was implemented in the POD model as a set of snapshots for each investigated operating point.

3. Reduced-order Model

The mathematical formulation of POD-RBF-ROM is presented in the following section. At first, the description of the POD-RBF model together with the implementation of the CFD results was given in Section 3.1. The proposed POD approximation basis was built using the Karhunen-Loève transformation approach employing Sirovich snapshot technique [35]. The RBF interpolation mathematical formula and integration with the POD model was described in Section 3.2.

3.1. Proper orthogonal decomposition model

The POD approach to constructing the optimal approximation base is built on the set of N sampled values of the two-phase flow parameters inside the ejector stored in a single vector called the snapshot [25]. Hence, the snapshot rectangular matrix $\mathbf{U}$ is generated for M snapshot vectors related to the number of the operating points (being the input parameters used to generate the snapshots). Snapshot vectors related to the number of operating points (being the input parameters used to generate the snapshots). The aim of the POD model is to define the orthogonal matrix Φ by reconstructing the basis snapshot matrix $\mathbf{U}$ based on the linear combination of the snapshots:

$$\Phi = \mathbf{U} \cdot \mathbf{V} \tag{6}$$

where $\mathbf{V}$ is the modal matrix defined in the following eigenvalue problem as a nontrivial solution:

$$\mathbf{C} \cdot \mathbf{V} = \Lambda \cdot \mathbf{V} \tag{7}$$

where Λ is the diagonal matrix and $\mathbf{C}$ is the positive covariance matrix. The covariance matrix can be defined as follows:

$$\mathbf{C} = \mathbf{U}^T \cdot \mathbf{U} \tag{8}$$

where $\mathbf{U}^T$ is a transpose snapshots matrix. In this situation, when the covariance matrix is known, the POD basis can be computed directly by solving an eigenvalue problem:

$$\mathbf{C} \cdot \phi^i = \lambda_i \cdot \phi^i \tag{9}$$

where ϕ^i is the orthogonal POD basis vector and λ_i is the eigenvalues stored by the diagonal matrix Λ. In the Karhunen-Loève transformation technique, the real and positive eigenvalues should be sorted in a descending order. The snapshots are strongly correlated with each other when the eigenvalues decrease rapidly due to increase of the mode number. Therefore, the POD model is able to use only part of the POD modes to obtain a high accuracy approximation. The *truncated* POD model $\bar{\Phi}$ considers $K < N$ elements for M operating points, which decreases the orthogonal matrix $\bar{\Phi}$ size.

$$\bar{\Phi} = \mathbf{U} \cdot \bar{\mathbf{V}} \tag{10}$$

where $\bar{\mathbf{V}}$ is the truncated modal matrix with first K eigenvectors of covariance matrix $\mathbf{C}$. The truncated POD basis is orthogonal and achieves optimal approximation properties. Moreover, there is no other approximation base having the same accuracy within a given approximation order. The snapshot reconstruction based on the truncated approximation formula needs to be done depending on additional parameters used in the snapshot generation. Hence, an arbitrary snapshot can be defined as follows:

$$\mathbf{u}^j \approx \sum_{k=1}^{K} \bar{\Phi}^k \alpha_k^j \tag{11}$$

where $\mathbf{u}^j$ is the vector of the arbitrary snapshot, $\bar{\Phi}^k$ is the k-element of the truncated orthogonal basis and α_k^j is the unknown coefficient vector related to the parameters used to create the snapshots. The foregoing approximation is valid only for snapshots used to build the POD basis. In the situation where the two-phase ejector is utilised in a wide range of the motive nozzle, suction nozzle and outlet operating conditions, the POD model requires an additional interpolation procedure to evaluate the ejector behaviour out of the operating points chosen in the course of POD basis construction.

3.2. Radial basis function interpolation

Based on the arbitrary snapshot equation presented in Eq. (11), the snapshot matrix $\mathbf{U}$ can be defined as a linear combination of the truncated POD vectors:

$$\mathbf{U} = \bar{\Phi} \cdot \bar{\alpha} \tag{12}$$

where $\bar{\alpha}$ is the unknown constant coefficients matrix, which can be computed as the transpose matrix of the orthogonal truncated POD basis Φ^T multiplied by the snapshot matrix:

$$\bar{\alpha} = \bar{\Phi}^T \cdot \mathbf{U} \tag{13}$$

In proposed ROM, the unknown coefficients matrix $\bar{\alpha}$ was defined as a non-linear function of the input parameters. Therefore, the foregoing coefficients matrix can be defined as follows:

$$\bar{\alpha} = \mathbf{B} \cdot \mathbf{F} \tag{14}$$

where $\mathbf{B}$ is the matrix of the unknown coefficients of the selected combination and $\mathbf{F}$ is the matrix of the interpolation functions $f_i\left(k - k^i\right)$ for the set of k parameters identical to the values used to build the subsequent snapshots. The radial basis interpolation functions were applied for the presented ROM as the RBF interpolation is mostly used for multidimensional approximation. In this study, the inverse multi-quadric radial function was employed due to the successfully implementation into the POD model in the literature [25, 36]. The mentioned interpolation function for i^{th} step is defined as follows:

$$f_i\left(|k-k^i|\right)=\frac{1}{\sqrt{\left(|k-k^i|\right)^2+r^2}} \tag{15}$$

where $|k-k^i|$ is the distance between the current set of the parameters k and the reference set of the parameters k^i, r is the smoothing factor. Considering the foregoing definition of the i^{th} interpolation function, the matrix **F** takes the following form:

$$\mathbf{F}=\begin{bmatrix} f_1\left(|k^1-k^1|\right) & \cdots & f_1\left(|k^j-k^1|\right) & \cdots & f_1\left(|k^M-k^1|\right) \\ \vdots & & \vdots & & \vdots \\ f_i\left(|k^1-k^j|\right) & \cdots & f_i\left(|k^j-k^j|\right) & \cdots & f_i\left(|k^M-k^j|\right) \\ \vdots & & \vdots & & \vdots \\ f_M\left(|k^1-k^M|\right) & \cdots & f_M\left(|k^j-k^M|\right) & \cdots & f_M\left(|k^M-k^M|\right) \end{bmatrix} \tag{16}$$

After the generation of the **F** matrix, the matrix **B** defined in Eq. (14) can be computed by use of the singular value decomposition technique [36]. Finally, the snapshot generation by use of the arbitrary parameter set k can be defined by the following equation:

$$\mathbf{u}^a(k)\approx\bar{\Phi}\mathbf{B}\mathbf{f}^a(k) \tag{17}$$

where $\mathbf{u}^a(k)$ is the calculated snapshot based on the arbitrary parameter set k and $\mathbf{f}^a(k)$ stands for column vector of interpolation functions defined in Eq. (15). The implementation of RBF into the POD model reduces the dimensionality of ROM to the number of unknown parameters k. The unknown parameters are defined as the boundary conditions of the CO_2 two-phase ejector. Therefore, the operating regimes selected to build the POD-RBF model as well as operating points between the POD-RBF model training points used for the validation procedure need to be defined.

4. Reduced-order Model Generation and Validation Procedure

The POD-RBF-ROM of the CO_2 two-phase ejector was built on the numerical results defined as a set of snapshots at selected operating points. Each snapshot contained the set of the local two-phase flow parameters for the ejector domain given by the CFD post-processing in the *ejectorPL* platform. In this paper, the POD-RBF approach was presented for single R744 two-phase ejector. ROM of the different ejectors can be generated individually for each ejector geometry configuration. Therefore, the results of each single ejector CFD model need to be used to generate ROM of the selected two-phase ejector at defined operating regime. The operating conditions, used to generate the POD base points, are presented in Section 4.1. The selection of the proper variables to generate the snapshots is described in Section 4.2. Finally, the numerical and the ROM experimental validation procedure is presented in Section 4.3.

4.1. Operating conditions of the reduced-order model

The defined operating conditions allow one to generate the POD basis model on the numerical results of the R744 ejector. Therefore, the selection of the two-phase flow parameters to generate a snapshot matrix needs to be performed at the specified operating conditions. Fig. 2 presents the motive nozzle operating points on the CO_2 pressure-specific enthalpy diagram selected to build the POD model of the two-phase ejector based on the CFD results. The operating points were defined for three constant motive nozzle temperatures of 25°C, 30°C and 35°C. Moreover, the pressure difference between the selected CFD points was set to 1 bar in the range from 70 to 100 bar based on the authors simulation and experimental investigation. The selected CFD operating points sampling

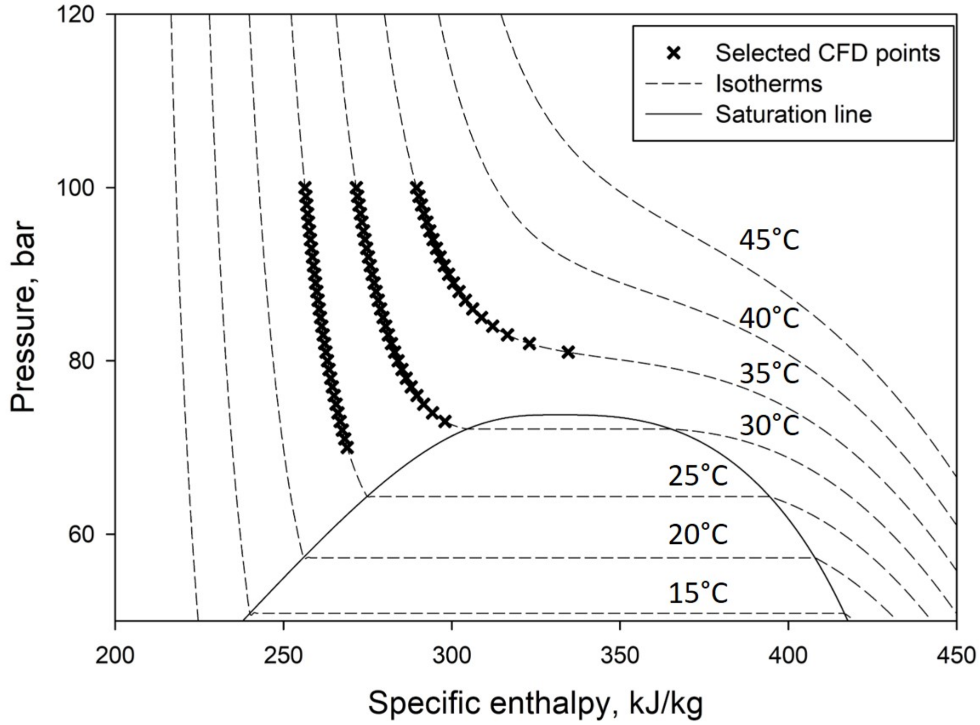

Figure 2: CO_2 pressure-specific enthalpy diagram with the motive nozzle operating points selected to generate the POD basis.

of 1 bar for 35°C was defined in the range from approximately 80 to 100 bar to cover the motive nozzle operating regime close to and above the critical point for which the HEM obtained high-accuracy CFD results.

All of the motive nozzle operating conditions presented in Fig. 2 were used to generate the POD model in combination with different suction nozzles and outlet operating conditions. Hence, the set of the selected suction nozzles and outlet conditions was presented in Table 2. The suction nozzle operating conditions were selected for two pressure levels, and the suction nozzle temperature was either at the vapour saturation state or with the assumed superheat of 15 K. In addition, the pressure difference between the ejector outlet and the suction nozzle (denoted as the pressure lift) was defined as 2 and 8 bars to obtain different ejector performance and entrainment possibilities for the motive stream. Therefore, each selected motive nozzle operating point was combined with four suction nozzle operating points at two different pressure lifts. The total number of the CFD ejector calculations used to generate the POD model was 630.

4.2. Snapshot processing

After the numerical calculations, all the CFD results of the selected operating points were exported as a snapshot vector. The size of the single snapshot depended on the number of variables taken into the consideration in the ROM. In the proposed model, the following two-phase flow parameters were used to generate the snapshot vector:

- Pressure
- Specific enthalpy
- Density
- Axial velocity

Table 2: The set of the suction nozzle and outlet operating conditions selected to generate the CFD-based POD model in combination with all motive nozzle operating points presented in Fig. 2.

No.	Suction nozzle		Outlet
	Pressure [bar]	Temperature [°C]	Pressure [bar]
OC_#1	28.00	-8.03	30.00
OC_#2	28.00	6.97	30.00
OC_#3	28.00	-8.03	36.00
OC_#4	28.00	6.97	36.00
OC_#5	32.00	-3.19	34.00
OC_#6	32.00	11.81	34.00
OC_#7	32.00	-3.19	40.00
OC_#8	32.00	11.81	40.00

- Radial velocity

The foregoing parameters enable the evaluation of the CO2 two-phase flow behaviour inside the investigated ejector. However, there are some possibilities for reducing the snapshot size and maintaining model accuracy. Based on the HEM assumption that the fluid properties can be calculated as a function of pressure and enthalpy given by the REFPROP libraries [31], the snapshot can be built on the pressure, specific enthalpy and velocity from the CFD results and the local density can be given by the foregoing libraries.

Moreover, the CFD results can be imported to the ROM either as a full ejector two-phase flow field, or as results obtained in the motive nozzle and the suction nozzle inlets. This reduction of the numerical results limited the mass flow rate calculations for each nozzle, which are the main output of the ROM for evaluating the energy performance of the R744 ejector-based refrigeration system in the dynamic simulations. For snapshots generated from the nozzle inlet CFD results, the ROM was able to take into account only the axial and radial velocity as the other parameters were defined by the operating conditions. Moreover, the snapshot can be generated only on the inlet nozzle and suction nozzle mass flow rates given by the CFD results.

The mentioned possibilities for generating the snapshots together with the total number of values in the single snapshot are presented in Table 3. The snapshot was generated in six combinations, depending on the parameter assumptions and investigated flow field. It can be seen that the total number of values considered in the snapshot significantly decreased by changing the investigated flow field area throughout the ejector field (Full in Table 3) into the inlet boundary fields (Bound. in Table 3). The six variants are defined in the following order:

- Variant #1 - considered pressure, specific enthalpy, density, and velocity fields given by the CFD results and the two-phase flow sampling was performed in the entire ejector CFD computational domain.
- Variant #2 - as in Variant #1, but the density field was excluded from the snapshot definition.
- Variant #3 - as in Variant #1, but the field values within the ejector are replaced with those on the inlet boundaries.
- Variant #4 - as in Variant #1, but the density field is excluded from the snapshot definition and the field values within the ejector are replaced with those on the inlet boundaries.
- Variant #5 - as in Variant #1, but the pressure, specific enthalpy, and density fields are excluded from the snapshot definition and the field values within the ejector are replaced with those on the inlet boundaries.
- Variant #6 - considered mass flow rates given by the CFD results from the inlet boundaries.

Table 3: The set of the snapshot generation combinations based on the CFD results.

Snapshot variant	Pressure	Specific enthalpy	Density	Axial velocity	Radial velocity	Flow field area	Number of values per snapshot
#1	CFD	CFD	CFD	CFD	CFD	Full	96,960
#2	CFD	CFD	-	CFD	CFD	Full	58,176
#3	CFD	CFD	CFD	CFD	CFD	Bound.	135
#4	CFD	CFD	-	CFD	CFD	Bound.	108
#5	-	-	-	CFD	CFD	Bound.	54
#6	Motive nozzle and suction nozzle mass flow rates					Bound.	2

The comparison of the snapshot generation combinations presented in Table 3 allowed one to find the best solution of the ROM in terms of the mass flow rate accuracy and computational time. Therefore, the validation procedure was performed to evaluate the ROM accuracy compared to the numerical results and the experimental data from the R744 vapour compression test rig equipped with the multi-ejector module given by SINTEF Energy Research in Trondheim, Norway. The multi-ejector module was developed in cooperation with the research institute SINTEF, academic university SUT and industrial partners DANFOSS and ENEX [37, 38].

4.3. Validation procedure

In the two-phase ejector the accuracy of the ROM results can be calculated as the relative error of the mass flow rates compared to either the numerical results or experimental data. The mass flow rate discrepancy was defined as follows:

$$\delta_i = 1 - \frac{\dot{m}_{i,ROM}}{\dot{m}_{i,REF}} \tag{18}$$

where $\dot{m}$ is the mass flow rate in kg/s, i is defined either motive nozzle or suction nozzle mass flow rate discrepancy, ROM is defined the mass flow rate obtained by ROM and REF is defined either CFD results or experimental data.

The validation procedure of the R744 two-phase ejector ROM was performed in the three following steps:

1. The POD-RBF-ROM approximation basis validation - the numerical results were compared to the results obtained from the POD-RBF model at the operating conditions selected to build ROM.
2. The POD-RBF-ROM validation based on the numerical results at the operating conditions chosen to fit areas that are not covered in the course of the snapshot generation.
3. The POD-RBF-ROM validation based on the experimental data at the operating conditions chosen to fit areas that are not covered in the course of the snapshot generation.

The POD basis validation was performed to confirm that the reduction of the CFD model into the POD model achieved high accuracy. Therefore, the operating conditions selected to build the POD model presented in Fig. 2 were used for the POD basis validation.

Fig. 3 presents the motive nozzle operating points selected to validate the ROM results compared to the numerical results. In addition, the POD operating points are shown. The investigated points were chosen to evaluate the ROM accuracy either for different pressure at similar temperature, or for similar pressure at different temperature, or both different pressure and temperature than the POD points. Moreover, the motive nozzle operating points were selected at an additional three constant temperatures of 27°C, 29°C, and 33°C to evaluate the ROM accuracy for both the systematic and random samples of the operating points.

In the numerically based validation procedure, the single suction nozzle and outlet conditions were defined to evaluate the accuracy of the ROM results between the operating points selected to build the POD model. Hence, the suction nozzle operating conditions and the pressure lift were defined as follows:

- The suction nozzle pressure was 30 bar,
- The suction nozzle temperature was -2.65°C,
- The outlet pressure was 35 bar.

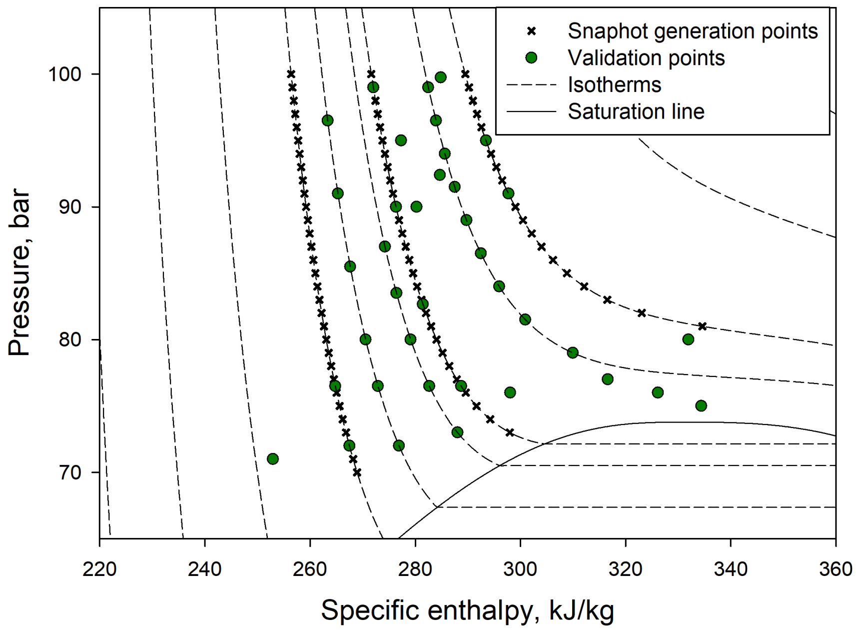

Figure 3: CO_2 pressure-specific enthalpy diagram with the motive nozzle operating points selected to the CFD-based validation procedure together with the POD operating points.

The motive nozzle operating points of the experimentally based validation procedure are shown on the pressure-specific enthalpy diagram in Fig. 4. Apart from the experimental operating points, the POD operating points are presented in this figure. Similar to the numerically based validation procedure, the investigated points were selected to evaluate the mass flow rate discrepancy of the ROM for the operating points that are chosen in between the training points. The experimental points were defined in three groups related to the pressure lift. Therefore, the experimental results with the pressure lift in the range of 2 to 4 bars was denoted as Low P_{lift} in Fig. 4. For the pressure lift in the range from 4 bar to 6 bar, the experimental results were named as Medium P_{lift}. Finally, the experimental points in the range from 6 bar to 8 bar were denoted as High P_{lift} allowing one to fully evaluate the ROM accuracy between the operating conditions used to build the POD-RBF basis. Each combination of different pressure lifts with the motive nozzle conditions covered the operating regimes of the ejector.

Fig. 5 presented the suction nozzle operating points in terms of different suction nozzle superheat and different pressure levels selected to perform the experimentally based ROM validation. Similar to the motive nozzle points presented in Fig. 4, each suction operating point is defined by three pressure lift values. The suction pressure level was set in the range from approximately 28 bar to over 32 bar related to the operating points selected to build the POD basis. The suction nozzle temperature is defined by the superheat in the range from 2 K to 12 K. Although most operating points were set with the suction nozzle superheat in the range from 8 K to 12 K.

Finally, the validation process of the ROM was defined to evaluate the accuracy of the proposed ROM. The motive nozzle and the suction nozzle discrepancies of each ROM result with different snapshot structures were compared to either the numerical results or experimental data. In addition, the numerically based validation allowed one to evaluate the accuracy of the ROM flow field results inside the R744 two-phase ejector.

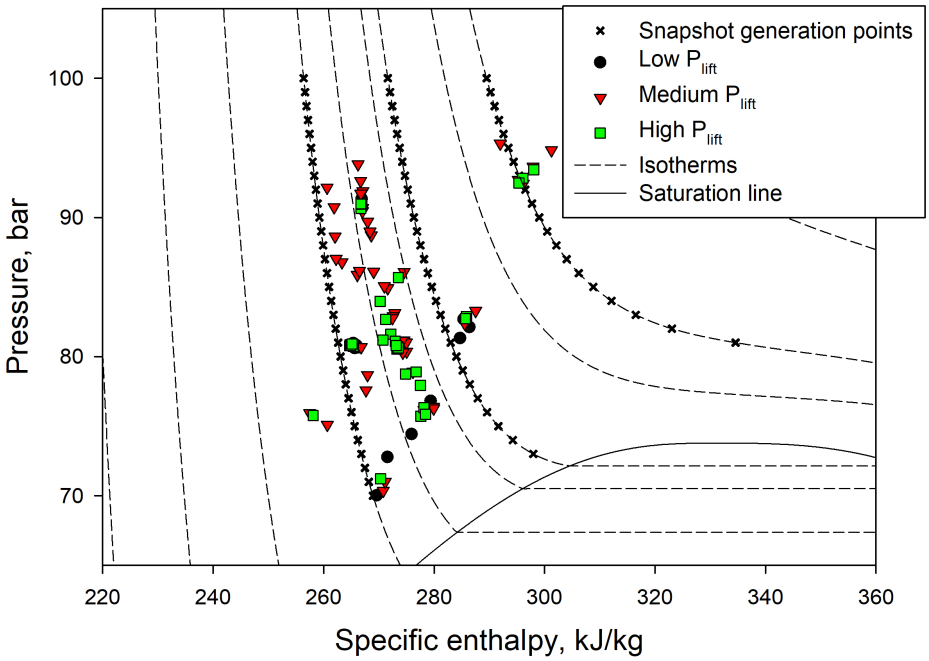

Figure 4: CO_2 pressure-specific enthalpy diagram with the motive nozzle operating points selected to the experimental-based validation procedure together with the POD operating points.

5. Results and discussion

All the obtained POD-RBF-ROM results are discussed in Section 5. In Section 5.1, the POD-RBF model validation is presented for each snapshot structure defined in Section 4.2. The results of the ROM numerical-based validation are shown in Section 5.2 and the ROM experimental-based validation results are presented in Section 5.3. Finally, the comparison of the computational time of each numerical and ROMs is discussed in Section 5.4.

5.1. The POD-RBF approximation basis validation

The validation procedure let one define the proper choice of input data for generating the POD-RBF approximation basis and evaluating the quality of the ROM results at the selected operating points defined in Section 4.1. The POD-RBF models Variant #1 and #2 were verified on the full flow field numerical results of the CO_2 two-phase ejector and the mass flow rate discrepancies. The accuracy of the motive and suction nozzle mass flow rates obtained from each ROM was investigated and compared to the CFD results.

Fig. 6 presents the R744 two-phase flow field of the absolute pressure, specific enthalpy and density inside the two-phase ejector given by the numerical model and Variant #1. The presented results were obtained for the motive nozzle pressure of 71 bars and a temperature of 25°C. The suction nozzle together with the outlet conditions were defined as OC_#1 in Table 2. Variant #1 obtained similar pressure distribution in the motive nozzle and the suction nozzle compared to the CFD results. In the pre-mixing and the constant-area mixing section, Variant #1 reached the same pressure distribution as the numerical model. In addition, the same pressure level in the diffuser was obtained by the CFD model and Variant #1.

Similar to the comparison of the absolute pressure results presented in Fig. 6(a), the similar local values of the R744 specific enthalpy were obtained in Variant #1 when compared to the CFD results in Fig. 6(b). The specific enthalpy of the motive stream decreased after the throat to approximately 250 kJ/kg in both models. The similar results for absolute pressure and the specific enthalpy throughout the R744 two-phase ejector allowed one to obtain the comparable mass flow rates of both streams compared to the numerical results. Therefore, the flow

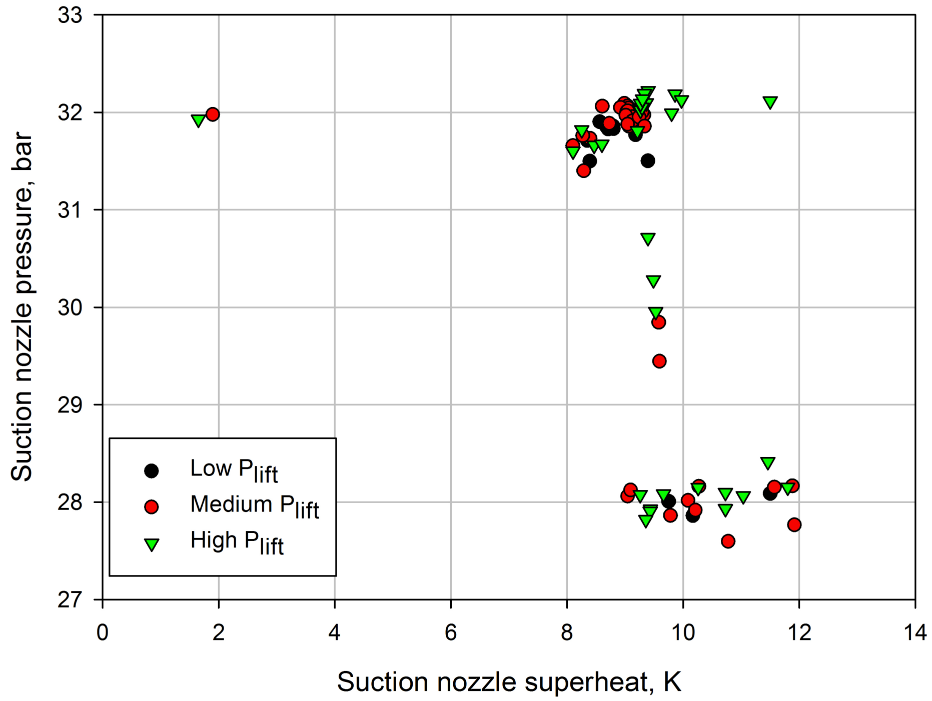

Figure 5: The suction nozzle operating points in terms of the suction nozzle superheat and pressure level for different pressure lift selected to the experimental-based validation procedure.

conditions in both nozzles were achieved in Variant #1. Finally, the density field obtained in Variant #1 and presented in Fig. 6(c) was similar to the CFD results for each ejector section. It can be seen that Variant #1 obtained the same density drop in the pre-mixer of approximately 100 kg/m^3 when compared to the CFD model. Therefore, the Variant #1 results of the two-phase flow inside the R744 ejector reached the same results in both nozzles, the pre-mixing and mixing sections and the diffuser compared to the CFD results. Therefore, the foregoing ROM enabled a similar mass flow rate to be achieved for each nozzle as the numerical model at the specified operating points selected to build the basis of the ROM.

Fig. 7 presents the R744 two-phase flow field results for the absolute pressure, specific enthalpy and density inside the two-phase ejector given by the numerical model and Variant #2. The results were obtained for the motive nozzle pressure of 90 bar and temperature of 30°C. The suction nozzle together with the outlet conditions were defined as OC_#5 in Table 2. The results obtained by Variant #2 were similar to the CFD results. The absolute pressure field of Variant #2 was slightly different than the CFD absolute pressure field close to the tip wall above the motive nozzle outlet position. In the specific enthalpy field presented in Fig. 7(b), the CFD model produced a small decrease of the specific enthalpy value at the end of the mixer close to the axis position that was omitted by the Variant #2 model. Both the foregoing differences did not influence the density field results given by both models and the Variant #2 model achieved the same density of R744 throughout the two-phase ejector compared to the CFD results. Therefore, it can be summarised that Variant #2 achieved high accuracy results when compared to the CFD results inside the R744 two-phase ejector at the operating conditions selected to build the ROM.

The motive nozzle mass flow rate accuracy for each ROM compared to the CFD results at the operating conditions is presented in Fig. 8. The motive nozzle mass flow rate obtained by the numerical model was compared for each ROM. Variants #1 and #2 indicated the same motive mass flow rate when compared to the CFD model. A similar high accuracy for the motive nozzle mass flow rate was obtained in Variants #3 and #4. The motive nozzle mass flow rates obtained by the Variants #5 and #6 ROMs were similar to the CFD results. Thereby each ROM

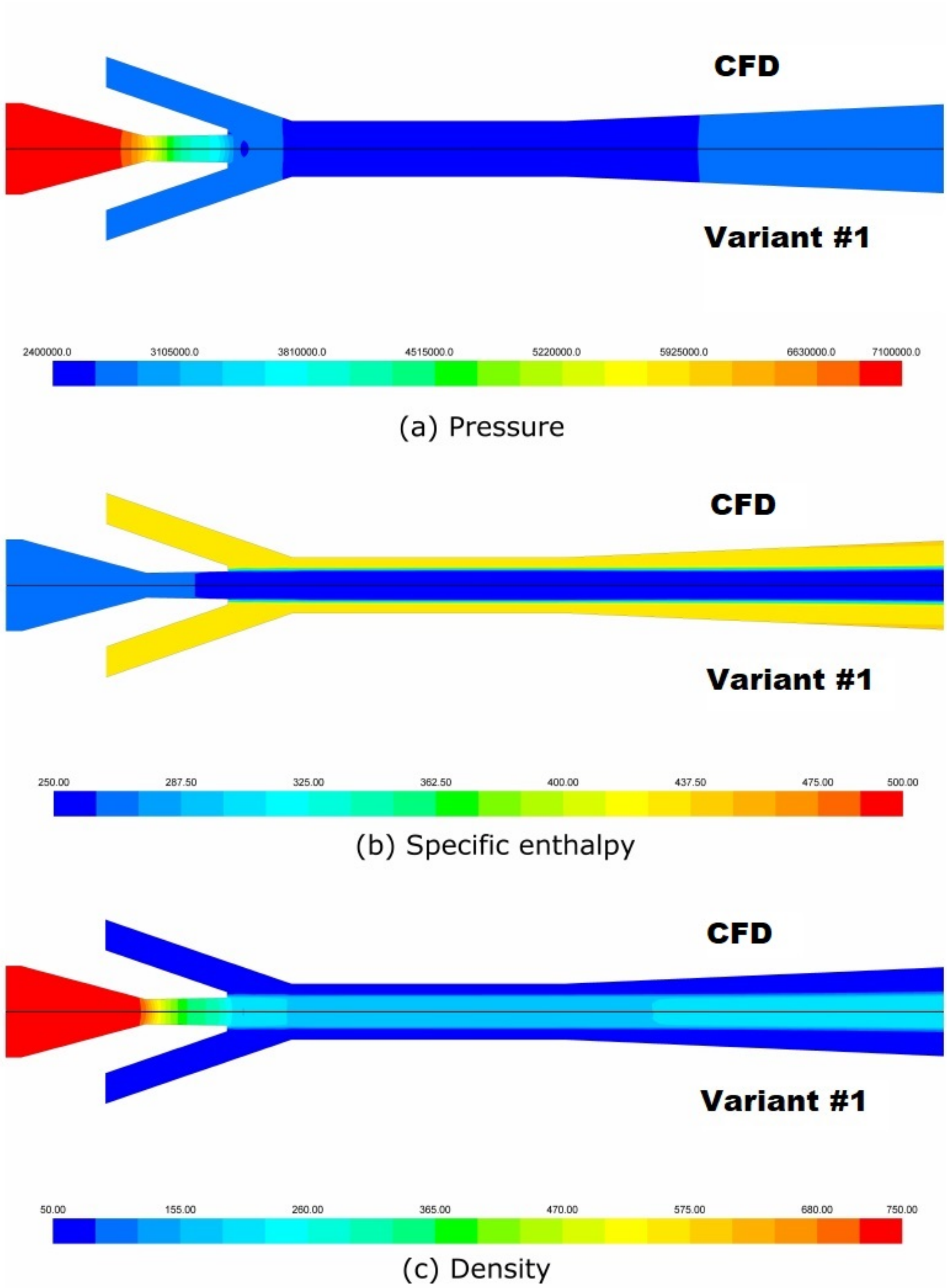

Figure 6: Results comparison between the CFD model (top) and Variant #1 (bottom) at the motive nozzle pressure of 71 bar and temperature of 25°C and the suction nozzle and outlet conditions denoted as # 5 in Table 2: (a) absolute pressure, (b) specific enthalpy and (c) density.

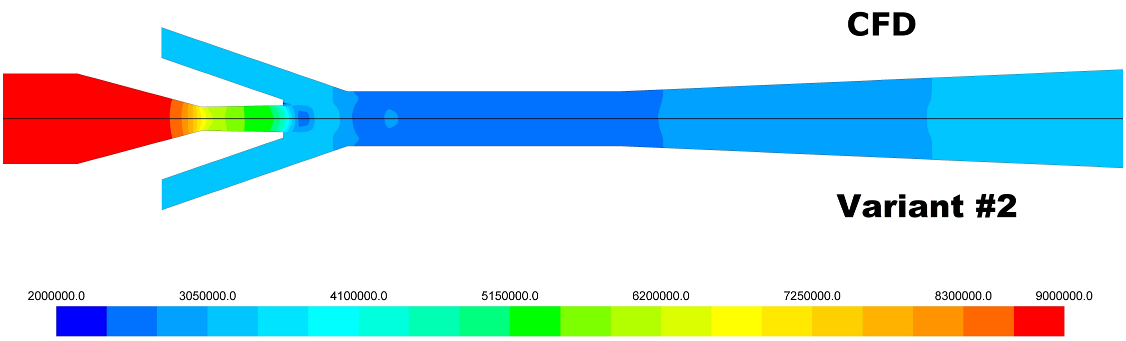

(a) Pressure

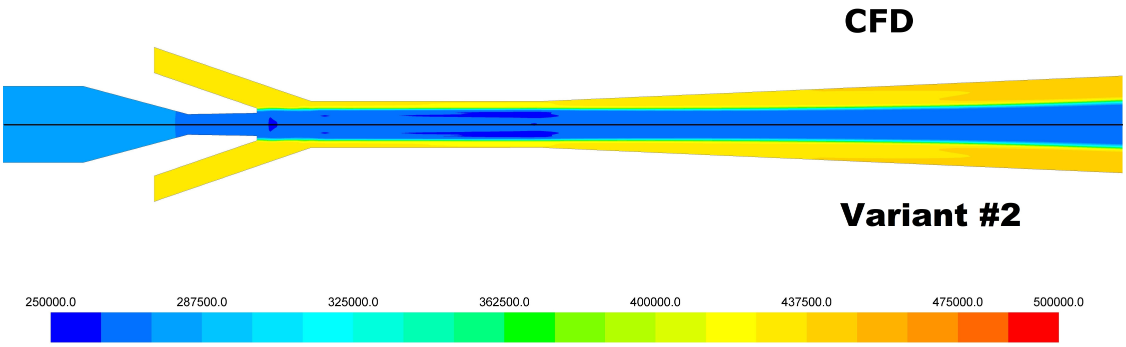

(b) Specific enthalpy

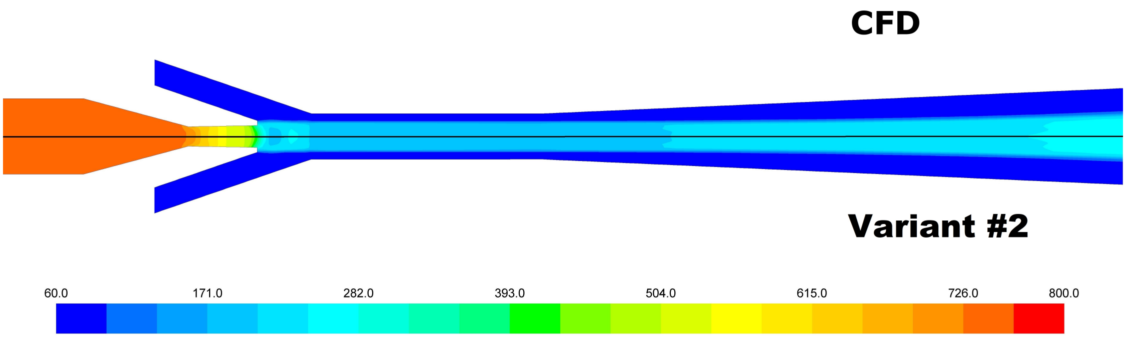

(c) Density

Figure 7: Results comparison between the CFD model (top) and Variant #2 (bottom) at the motive nozzle pressure of 90 bar and temperature of 30°C and the suction nozzle and outlet conditions denoted as # 5 in Table 2: (a) absolute pressure, (b) specific enthalpy and (c) density.

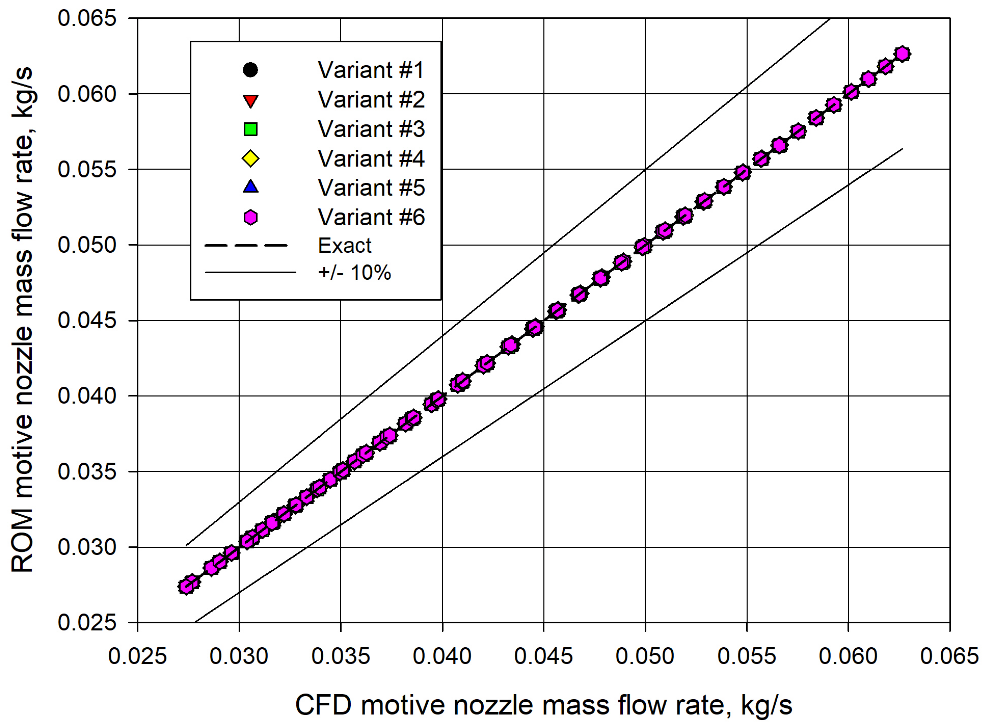

Figure 8: The motive nozzle mass flow rate given by ROM and the CFD model at the operating conditions presented in Fig. 2.

reached a negligible discrepancy for the motive nozzle mass flow rate at the operating points presented in Section 4.1.

Fig. 9 presents the suction nozzle mass flow rate accuracy for each ROM compared to the CFD results at the selected operating conditions. Similar to the motive nozzle mass flow rate results presented in Fig. 8, Variants #1 and #2 reached a similar mass flow rate for the suction stream as obtained in the CFD model. Moreover, Variants #3, #4, #5 and #6 obtained very high accuracy within ±1% of the suction nozzle mass flow rate. Each investigated ROM obtained the same CO2 motive nozzle and suction nozzle mass flow rates compared to the numerical results. Hence, the POD-RBF approximation basis of each ROM correctly reproduces the numerical results of the R744 two-phase ejector.

The POD-RBF approximation basis validation confirmed that each ROM is characterised by high accuracy of the motive nozzle and the suction nozzle mass flow rates when compared to the CFD results. Moreover, Variants #1 and #2 reached the same results for the R744 two-phase flow parameters inside the two-phase ejector as the numerical model. Therefore, the validation procedure at the operating points defined in Sections 5.2 and 5.3 allowed one to evaluate the accuracy of the RBF interpolation in each ROM.

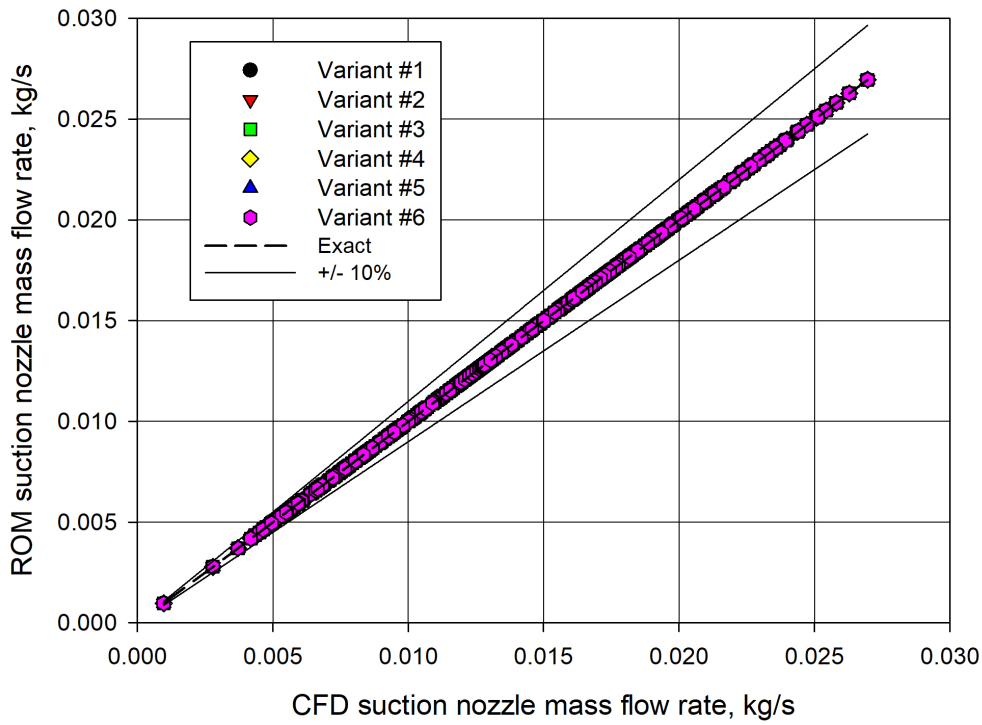

Figure 9: The suction nozzle mass flow rate given by ROM and the CFD model at the operating conditions presented in Fig. 2.

5.2. The POD-RBF-ROM numerical-based validation

The operating conditions specified in Section 4.3 let one evaluate the accuracy of the proposed R744 two-phase ejector ROM between the base points. The two-phase flow field analysis and the mass flow rate discrepancy for each ejector nozzle obtained by the ROMs were compared to the CFD results.

Fig. 10 presents the absolute pressure of the R744 two-phase flow inside the two-phase ejector. The results were obtained on the basis of both Variants #1 and #2. In this figure, the CFD results were also introduced to compare the pressure field inside the ejector with the ROM results. The motive nozzle pressure and temperature were set as follows: 99 bar and 30°C in Fig. 10(a), 80 bar and 34.4°C in 10(b), 71 bar and 21°C in 10(c), respectively. The suction nozzle and the outlet operating conditions were set according to the operating points presented in Section 4.3. It can be seen in Fig. 10(a) that the pressure field for both ROMs was similar to the CFD results in the motive nozzle, suction nozzle, pre-mixer, and the ending part of the diffuser. In similar, the satisfactory prediction of the pressure distribution was obtained for Variants #1 and #2 in Fig. 10(b). The ROMs pressure field with small differences in the mentioned ejector sections let to predict the motive nozzle and suction nozzle mass flow rates comparable to the CFD model. In situation presented in Fig. 10(c), both ROMs overestimated the motive nozzle pressure field when compared to the CFD results due to the selected motive nozzle operating conditions outside of the defined ROM operating regime presented in Section 4.1. Hence, the ROM Variants #1 and #2 for the foregoing operating conditions was not able to predict motive nozzle mass flow rate in similar way to the CFD model regarding to the pressure differences in the motive nozzle. The presented results show that ROM can be applied only within the defined operating regime to predict the two-phase flow fields with the satisfactory accuracy.

The motive nozzle mass flow rate accuracy for each ROM compared to the CFD results at the operating conditions presented in Fig. 3 is shown in Fig. 11. It can be seen that each ROM obtained a notably low discrepancy of the motive nozzle mass flow rate for most of the investigated operating points. An accuracy for Variants #3 and #4 within ±10% was reached for the motive nozzle mass flow rate above 0.035 kg/s. For the CFD mass flow rate below 0.035 kg/s, the accuracy of mentioned ROMs was over 10% and mass flow rate was overestimated. The accuracy of Variant #5 was within ±10% above 0.03 kg/s. The motive mass flow rate accuracy of Variant #6 was within ±10% mass flow rate above 0.035 kg/s and below 0.035 kg/s Variant #6 overestimated of approximately 0.005 kg/s compared to the CFD model. It can be seen that each ROM overestimated the motive nozzle mass flow rate below approximately 0.045 kg/s and underestimated it above 0.045 kg/s. The satisfactory prediction of each ROM in the range from 0.035 kg/s to 0.06 kg/s confirmed that the POD-RBF approach keep the CFD model accuracy in the majority of the points located within the defined operating regime. The ROMs discrepancy above 10% for the motive nozzle mass flow rate below 0.035 kg/s resulted from the localisation of the operating conditions close to the critical point and outside the defined operating regime. Based on the results presented in Fig. 11 the best accuracy was obtained by Variant #5.

Fig. 12 presents the comparison of the suction nozzle mass flow rate given by the CFD results and the proposed ROMs. Similar to the results presented in Fig. 11, the ROM suction nozzle mass flow rate accuracy was performed at the operating conditions presented in Section 4.3. The discrepancy of the suction nozzle mass flow rate reached by ROMs was within ±10% in the range from approximately 0.014 kg/s to 0.019 kg/s. The suction mass flow rate overestimation of Variant #3 above 10% was below 0.014 kg/s. In addition, Variant #3 underestimated the suction mass flow rate above 0.019 kg/s with an accuracy of below -10%. The accuracy of Variants #4, #5 and #6 was similar to Variant #3 below 0.014 kg/s. Moreover, the mentioned ROMs underestimated the mass flow rate of the suction stream compared to the numerical model for the CFD suction mass flow rate over approximately 0.018 kg/s. The highest discrepancy of the suction mas flow rate of approximately -15% was obtained for Variants #3, #4, and #6 for the suction mass flow rate of approximately 0.021 kg/s, and Variant #5 for the mass flow rate of approximately 0.011 kg/s. However, Variant #5 obtained the best accuracy for the suction mass flow rates above 0.018 kg/s. It can be seen that the suction nozzle mass flow rate was more sensitive parameter than the motive nozzle mass flow rate as the result of the RBF interpolation possibilities and the selected suction nozzle and outlet operating condition. However, the satisfactory discrepancy was obtained for most of the validated points. The high accuracy of each ROM case confirmed that the selected operating conditions for both nozzles and the outlet conditions for generating the POD-RBF approximation basis let one perform the calculation between the selected operating points with a low discrepancy for the suction nozzle mass flow rate.

The numerically based validation allowed one to evaluate each ROM accuracy at the operating points required by the RBF interpolation. The low POD-RBF-ROM discrepancies of the motive nozzle and the suction nozzle mass flow rates were reached due to the high number of the POD-RBF approximation basis generation points and the high accuracy RBF interpolation at the operating conditions selected for the foregoing validation procedure. The best accuracy for the motive and suction nozzle mass flow rates was obtained by Variant #5.

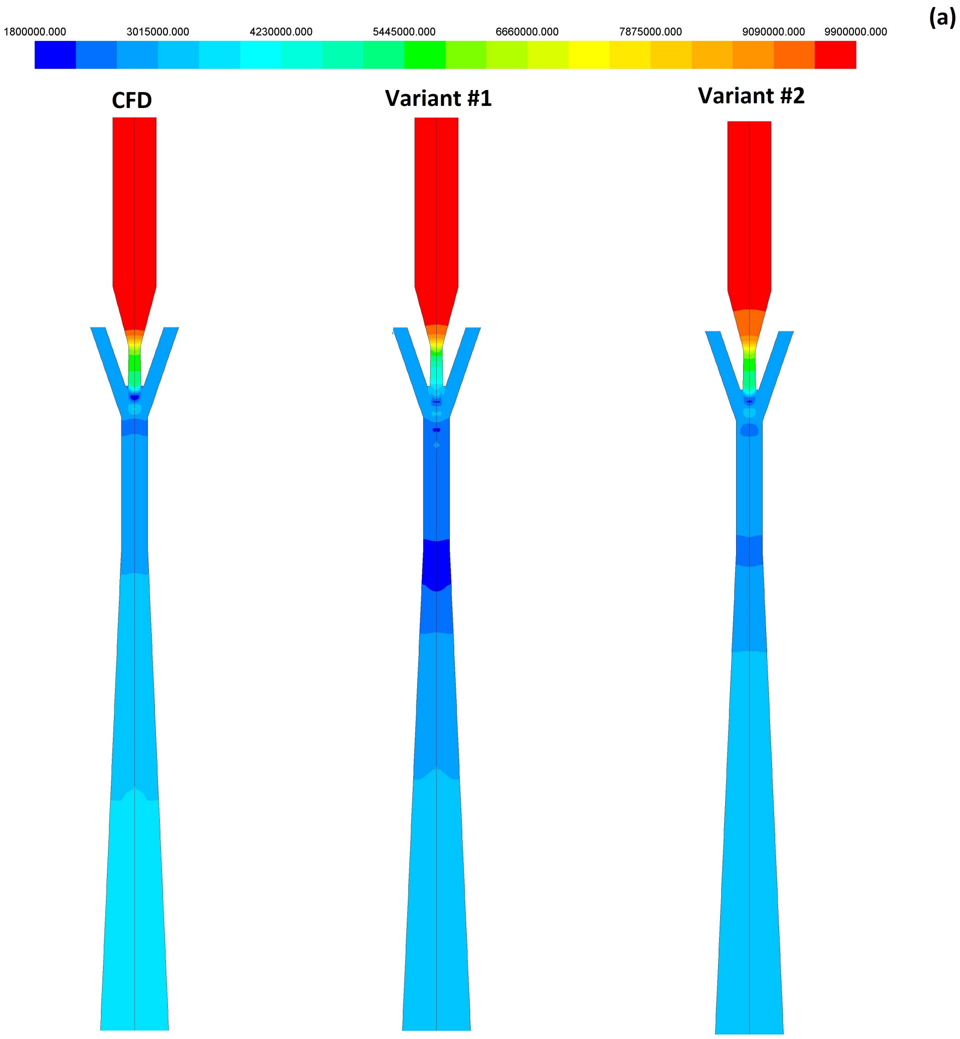

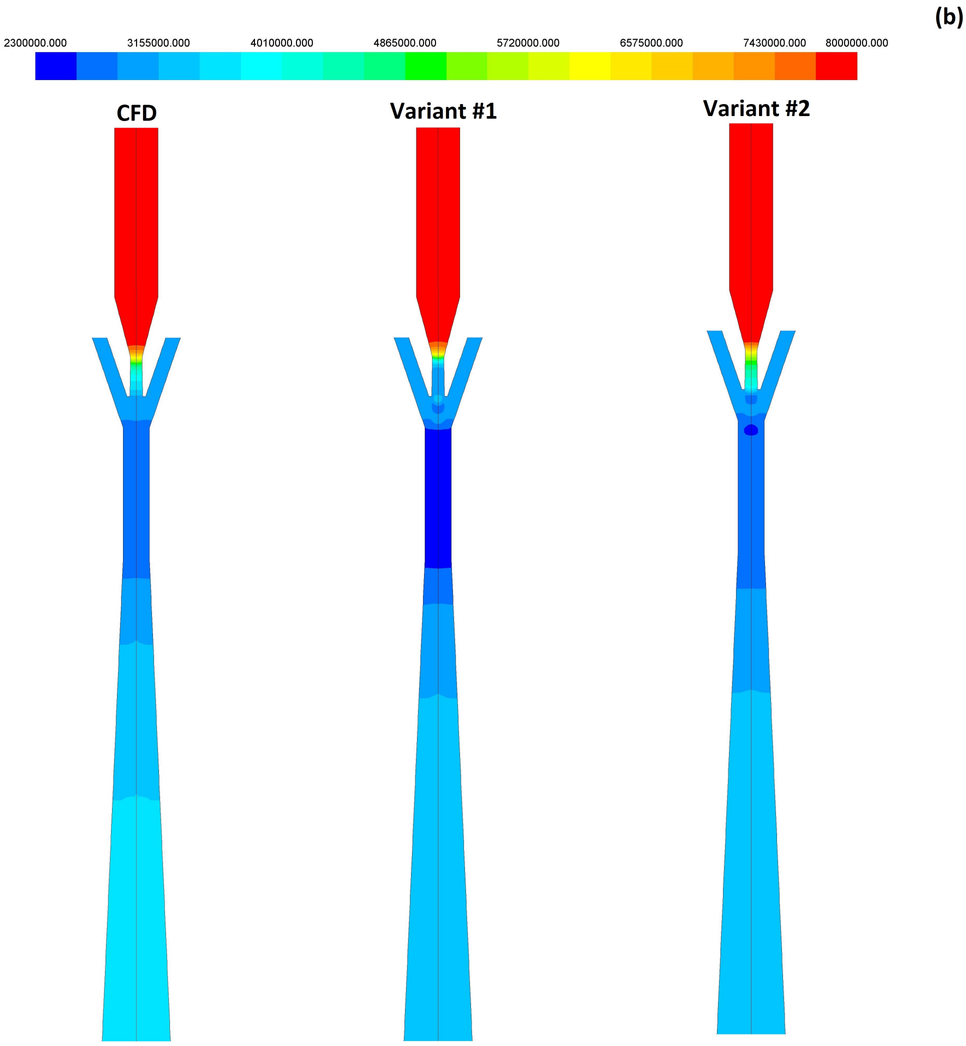
(b)
2300000.000
3155000.000
4010000.000
4865000.000
5720000.000
6575000.000
7430000.000
8000000.000
CFD
Variant #1
Variant #2

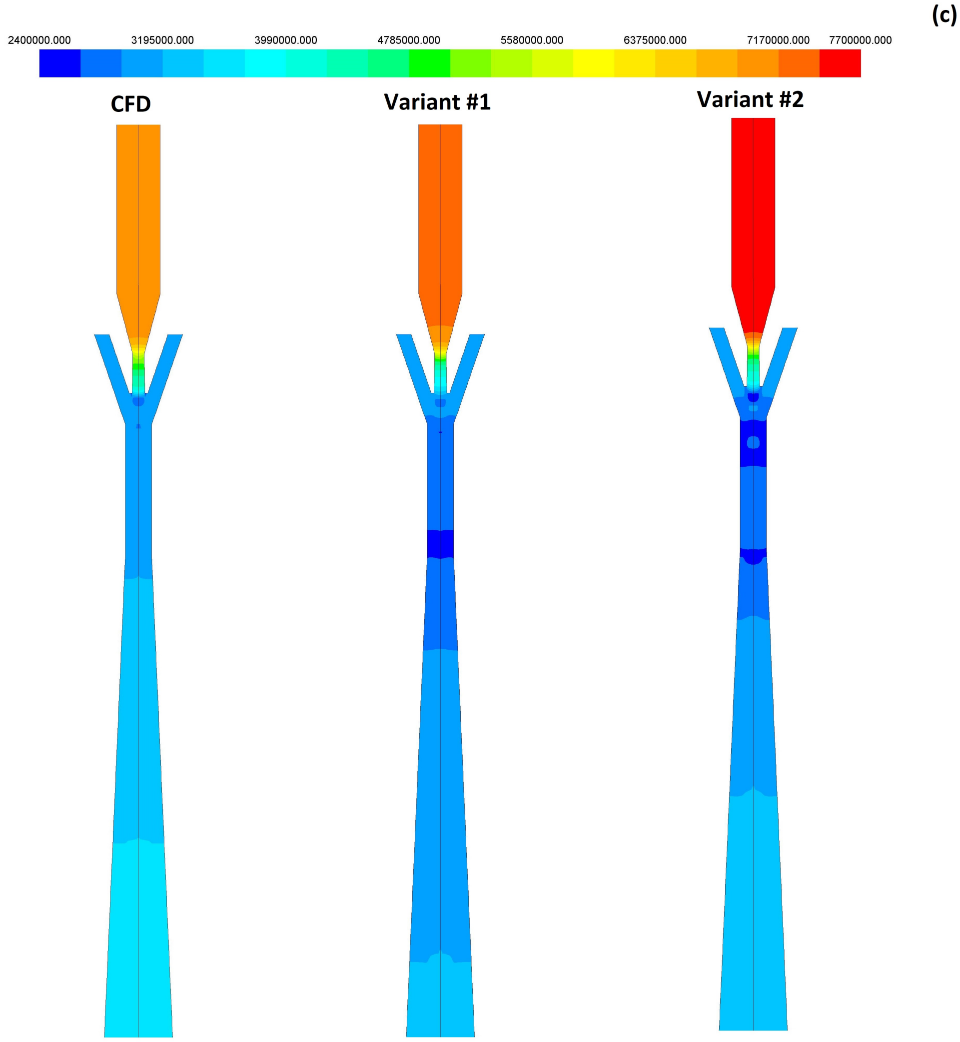

Figure 10: The absolute pressure of the R744 two-phase flow inside the ejector given by CFD results, Variant #1 and Variant #2 at the motive nozzle parameters: (a) pressure of 99 bar, temperature of 30°C; (b) pressure of 80 bar, temperature of 34.4°C; (c) pressure of 71 bar, temperature of 21°C. The suction nozzle together with the outlet conditions presented in Section 4.3.

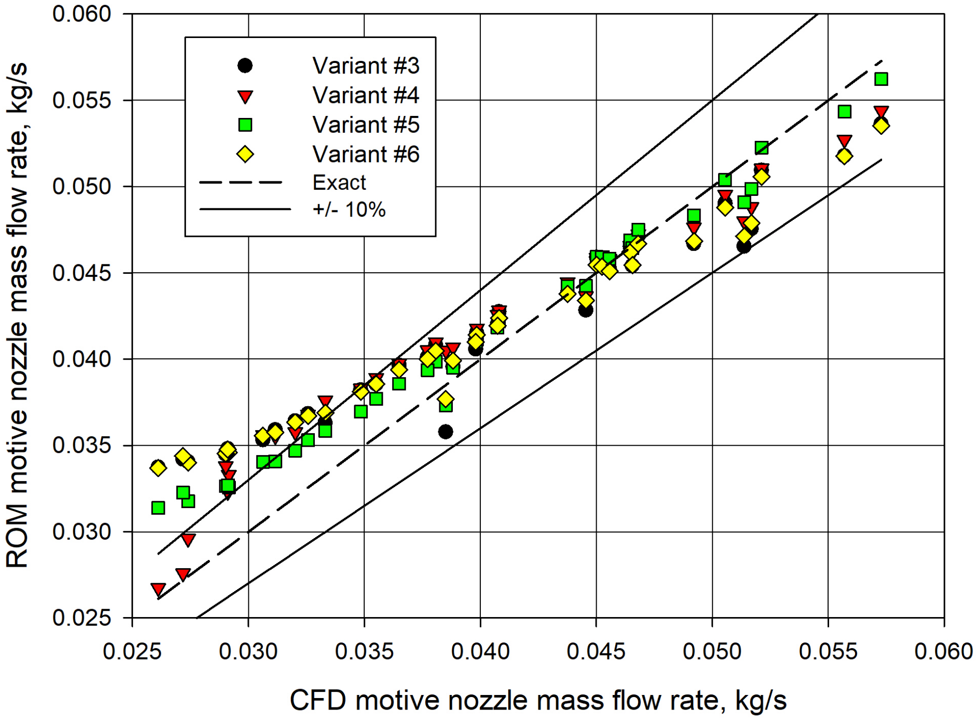

Figure 11: The motive nozzle mass flow rate given by ROM and the CFD model at the operating conditions presented in Fig. 3.

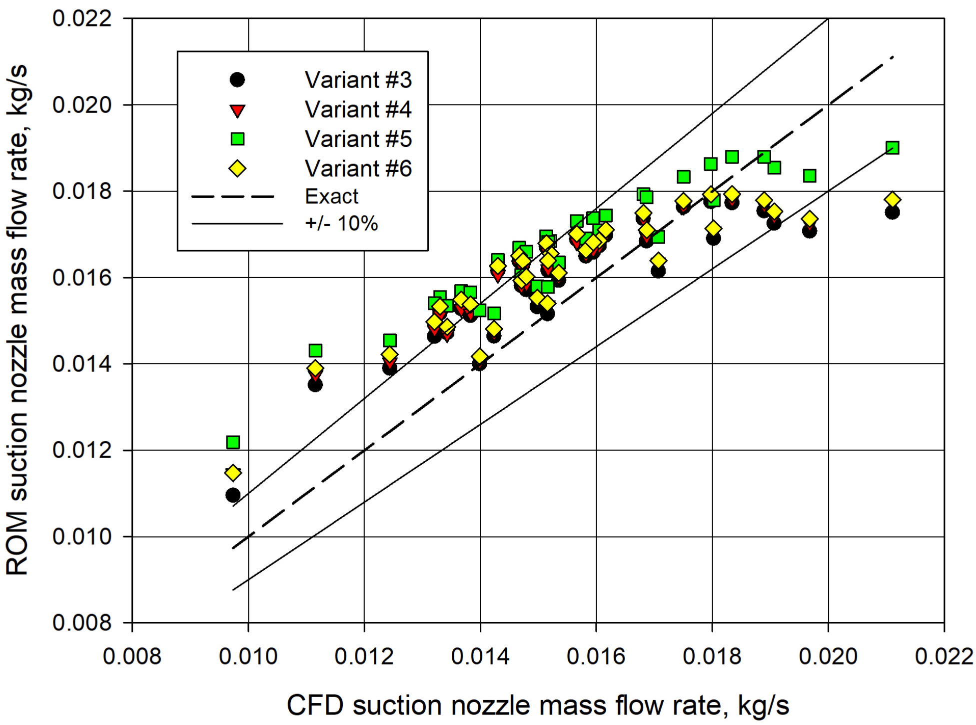

Figure 12: The suction nozzle mass flow rate given by ROM and the CFD model at the operating conditions presented in Fig. 3.

5.3. *The POD-RBF-ROM experimental-based validation*

The validation of each ROM based on the CFD results confirmed the high accuracy of the calculated mass flow rates for both the R744 two-phase ejector nozzles. Therefore, the experimentally based validation was performed to evaluate the discrepancies of the motive and suction nozzle mass flow rates obtained by ROM compared to the experimental data of the R744 two-phase ejector.

Fig. 13 presents the comparison of the motive nozzle mass flow rate given by the experimental data and each proposed ROM at the operating conditions presented in Fig. 4. It can be observed that the discrepancy of each ROM is within ±10% for nearly all investigated operating points. Variant #5 obtained slightly higher inaccuracy for high mass flow rate above approximately 0.054 kg/s. The motive nozzle mass flow rate for each ROM is underestimated for the mass flow rate over approximately 0.04 kg/s. The results given by Variants #3, #4 and #6 are within ±10% for each operating point selected for the experimental-based validation. The motive nozzle mass flow rate accuracy for Variants #3 and #6 are slightly below -10% for the mass flow rate of approximately 0.0475 kg/s. Hence, each ROM reaches a high accuracy for the motive nozzle mass flow rate compared to the experimental data. In addition, the best accuracy was obtained in Variant #6 and the lowest accuracy was reached in Variant #5 because of high underestimation for higher values of the motive mass flow rate. The unsatisfactory discrepancy of ROM Variant #5 for the motive nozzle mass flow rate above 0.054 kg/s was reached as a result of the RBF interpolation possibilities to predict the value of the motive stream. However, the satisfactory prediction of the ROMs motive nozzle mass flow rate was obtained for the defined operating regime typical for supermarket applications.

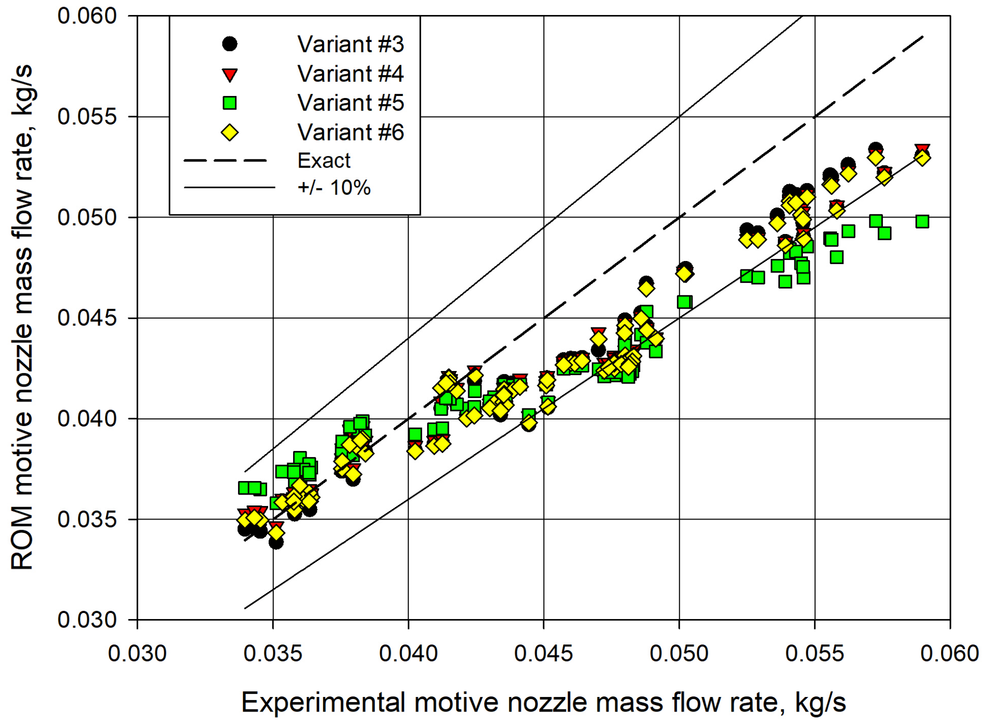

Figure 13: The motive nozzle mass flow rate given by ROM and the experimental data at the operating conditions presented in Fig. 4.

Similar to the results presented in Fig. 13, the ROM suction nozzle mass flow rate accuracy of the experimentally based validation procedure is shown in Fig. 14. The validation investigation was performed according to the operating conditions presented in Fig. 5. The suction nozzle mass flow rate discrepancy of each ROM was within ±10% for most investigated points. Moreover, the results obtained by each ROM were similar to each other. The highest discrepancy was obtained in Variant #5 for the suction nozzle mass flow rate of approximately 0.045 kg/s. This value means a mass flow rate underestimation by -100%. Hence, increasing of the POD-RBF approximation basis generated operating points with high pressure lift, as was required to improve the accuracy of the ROM results for very low suction nozzle mass flow rate. In addition, Variant #5 reaches inaccuracy above 15% for most results above approximately 0.014 kg/s. The ROMs discrepancy of the suction nozzle mass flow rate above ±10% was reached due to the high number of the operating conditions for which the suction nozzle pressure was above 32 bar or below 28 bar. Hence, the RBF interpolation was not able to predict the suction nozzle mass flow rate with satisfactory accuracy. Although, the ROMs accuracy of the suction nozzle was within ±15% for most of the investigated points, especially Variants #3, #4 and #6.

The experimentally based validation shows the high accuracy of the boundary flow field ROM. The results obtained for Variants #3 and #4 reached a high accuracy for the motive nozzle and suction nozzle mass flow rates. In addition, Variant #6 obtained a similar low discrepancy at most experimentally based operating conditions letting one evaluate the R744 two-phase ejector at high accuracy with minimum size of the POD-RBF model. Based on the experimentally based validation, Variant #5 requires increasing the selected CFD operating points to build the POD-RBF approximation basis for improving the accuracy of the suction nozzle mass flow rate.

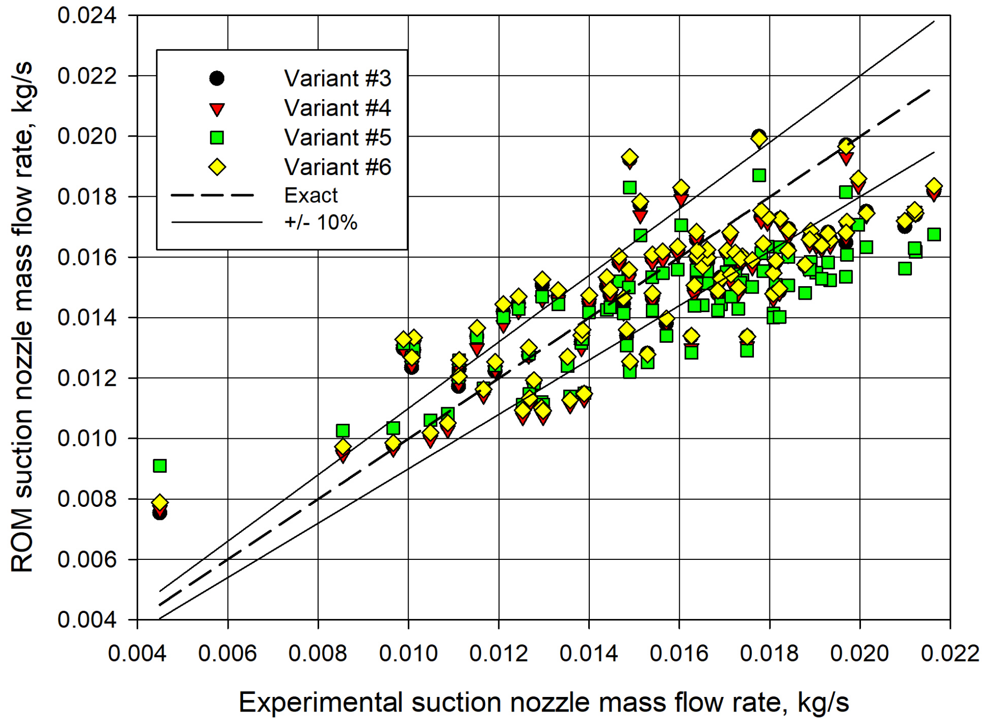

Figure 14: The suction nozzle mass flow rate given by ROM and the experimental data at the operating conditions presented in Fig. 5.

Fig. 15 presents the ROM Variant #6 motive nozzle and suction nozzle discrepancies under the operating conditions outside of the defined operating regime in Section 4.1. The ROM results were compared with the experimental data. The motive nozzle and suction nozzle operating conditions were shown in Fig. 15a and Fig. 15b, respectively. It can be seen that the motive nozzle temperature was either below 25°C or above 35°C and the suction nozzle superheat was above 8 K for each investigated operating point. Moreover, the pressure lift varied in the range from 4 bar to 8 bar. The ROM motive nozzle discrepancy was slightly above 0.1 for OC1 and OC2. Each mentioned operating point was outside the defined ROM operating regime and in the subcritical conditions, where the density of the subcooled liquid significantly increased during the decrease of the temperature. Hence, the ROM was not able to predict motive nozzle mass flow rate with the accuracy within 10%. However, the discrepancy of the motive nozzle mass flow rate for OC3 was approximately 0.08 as the temperature of the selected point was close to 25°C. The suction nozzle mass flow rate was of approximately 0.05 for OC3 and above 0.1 for OC1 and OC2. In situation, where the motive nozzle temperature was above the defined ROM operating regime, the motive nozzle mass flow rate discrepancy was approximately -0.03 for OC4, OC5 and OC6. The increase of the temperature in the transcritical conditions slightly decreased the motive nozzle mass flow rate, thereby ROM predicted the mass flow rate with high accuracy. However, the suction nozzle mass flow rate discrepancy for each mentioned operating point was above 0.1 as a result of the pressure lift and motive nozzle pressure influence on the entrainment possibility of the ejector. Therefore, ROM can be applied only within the defined operating regime to predict the motive nozzle and suction nozzle mass flow rates with acceptable accuracy.

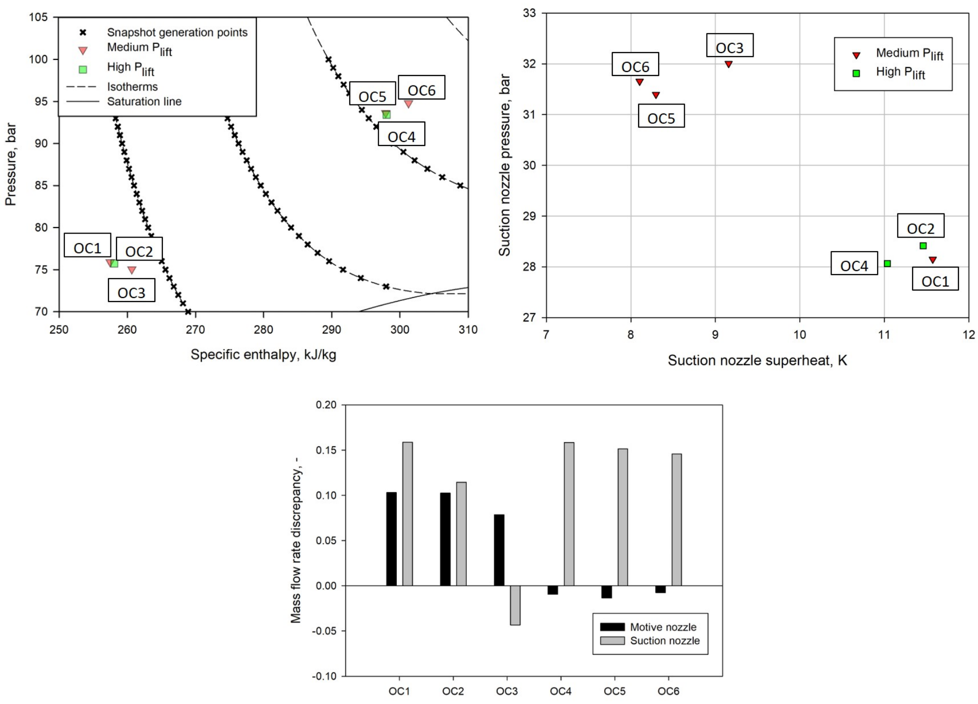

Figure 15: The ROM Variant #6 motive and suction nozzle mass flow rate discrepancy at the operating conditions outside the operating regime defined in Section 4.1: (a) R744 pressure-specific enthalpy diagram together with the motive nozzle operating conditions; (b) Suction nozzle operating conditions; (c) Mass flow rates discrepancies.

5.4. *Computational time*

The validation procedures presented in Section 4.3, 5.2 and 5.3 let to evaluate the accuracy of each investigated ROM. Apart from the information about the accuracy of the ROM results, the analysis of the computational time let to define the benefits to use ROM in the dynamic simulation. Therefore, set of the computational time of each model single case is presented in Table 4. It can be seen that the numerical model requires approximately thirty minutes to solve the single case of the R744 two-phase ejector. Variant #1 reduces significantly the computational time up to 11.61 s. The further reduction of the POD-RBF approximation basis let to compute the single case in approximately 2.00 s for Variant #2 and below 0.1 s for the boundary flow field ROMs. Variant #6 reaches the most reduction of the computational time up to 0.04 s. Therefore, ROM of the two-phase ejector can be implemented to the dynamic simulations of the refrigeration systems due to negligible influence on the computational time of the simulations.

Table 4: The set of the single case computation time of each numerical R744 two-phase ejector model.

Investigated model	Computational time
CFD model	≈ 1800 s
Variant #1	11.61 s
Variant #2	1.90 s
Variant #3	0.08 s
Variant #4	0.07 s
Variant #5	0.05 s
Variant #6	0.04 s

6. Conclusions

The proposed ROM of the R744 two-phase ejector was developed and validated. The numerical model of the CO_2 two-phase ejector based on the HEM fluid assumption was used to build the POD-RBF approximation basis for the ROM. The operating points were selected to achieve high accuracy CFD results for typical supermarket applications. The inverse multi-quadric radial interpolation function was employed to calculate the ejector performance between the operating points selected to build the POD-RBF approximation basis. In addition, the different snapshot generations were investigated to evaluate the best preparation of the ROM based on the validation procedures and time of the single case computation. The POD-RBF approximation basis with different snapshot sizes was validated at the selected POD generation operating points. The results of the POD-RBF-ROMs were compared with the numerical results and the experimental data. In addition, the computational time for each investigated model was analysed.

The POD-RBF approximation validation confirmed the high accuracy of each ROM. The discrepancy of the motive nozzle mass flow rate was within ±10% for all investigated ROMs. Similar to the motive nozzle mass flow rate discrepancy, the ROM suction nozzle mass flow rate accuracy was within ±10% at each investigated operating point. The R744 two-phase flow field results obtained for Variant #1 were similar to the results given by the CFD model. In addition, Variant #1 reached similar pressure, specific enthalpy and density fields as the CFD results. Therefore, the reduction of the snapshot size by omission of the fluid density inside the two-phase ejector let one achieve the high accuracy of the flow field results and mass flow rates of both ejector nozzles.

According to the flow field comparison between the CFD results and Variants #1 and #2 in the numerically based validation, the high discrepancy of the R744 flow field was obtained by both ROMs. Therefore, each foregoing ROM required increasing the number of the operating points to build the POD-RBF approximation basis for improving model accuracy. The rest of the ROMs obtained low discrepancy for the motive nozzle and suction nozzle mass flow rates within ±10% at most validated operating points compared to the numerical results. Hence, the selected RBF interpolation let one predict the proper mass flow rate for each R744 ejector nozzle within the POD-RBF approximation basis operating conditions.

A high accuracy of the motive nozzle mass flow rate was reached by each ROM for the experimental-based validation. The reduction of the snapshot into the boundary velocity profile in Variant #5 increased the model discrepancy for the high motive nozzle mass flow rate. However, the smallest Variant #6 established high accuracy similar to Variants #3 and #4. The same behaviour was obtained by Variant #6 for the suction nozzle mass flow rate experimentally based validation. Hence, the POD-RBF approximation basis generation based on the mass flow rates lets one evaluate the ejector performance at high accuracy at either the transcritical or subcritical operating conditions typical for supermarket applications.

The computational time analysis confirmed that the developed ROM significantly reduced the time to compute a single case. In addition, the results of the motive nozzle and suction nozzle mass flow rates at the selected operating conditions were provided by Variant #6 below 0.05 s. Therefore, the implementation of the ROM in the simulation analysis of the R744 ejector-based refrigeration system let one immediately reach the results of the ejector performance for a single time step.

The proposed ROM obtained high accuracy for most investigated points. However, the ROM can be improved by increasing the number of the CFD results implemented in the POD-RBF approximation basis as snapshots. In addition, the hybrid combination of the numerical model and the experimental data let one reach very high accuracy for the ROM motive nozzle and suction nozzle mass flow rates at a considerably more extended operational envelope, maintaining notably low computational time.

7. Acknowledgement

The authors gratefully acknowledge the financial support of the Research Council of Norway through project No. 244009/E20. The work of MP and JS was also partially supported by the Rector's research grant provided by SUT.

References

[1] U. N. E. Programme, O. Secretariat, Handbook for the montreal protocol on substances that deplete the ozone layer.
URL http://ozone.unep.org/new_site/en/montreal_protocol.php

[2] A. Pearson, Carbon dioxide—new uses for an old refrigerant, International Journal of Refrigeration 28 (8) (2005) 1140–1148. doi:http://dx.doi.org/10.1016/j.ijrefrig.2005.09.005.
URL http://www.sciencedirect.com/science/article/pii/S0140700705001660

[3] M. H. Kim, J. Pettersen, C. W. Bullard, Fundamental process and system design issues in co2 vapor compression systems, Progress in Energy and Combustion Science 30 (2) (2004) 119–174. doi:10.1016/j.pecs.2003.09.002.
URL http://www.scopus.com/inward/record.url?eid=2-s2.0-1042288940&partnerID=40&md5=937deb77622c2dd30ccb15349ae081e3

[4] V. Sharma, B. Fricke, P. Bansal, Comparative analysis of various co2 configurations in supermarket refrigeration systems, International Journal of Refrigeration-Revue Internationale Du Froid 46 (2014) 86–99. doi:DOI10.1016/j.ijrefrig.2014.07.001.
URL <GotoISI>://WOS:000345233500011

[5] A. Chesi, F. Esposito, G. Ferrara, L. Ferrari, Experimental analysis of r744 parallel compression cycle, Applied Energy 135 (0) (2014) 274–285. doi:http://dx.doi.org/10.1016/j.apenergy.2014.08.087.
URL http://www.sciencedirect.com/science/article/pii/S0306261914009106

[6] S. Elbel, P. Hrnjak, Experimental validation of a prototype ejector designed to reduce throttling losses encountered in transcritical r744 system operation, International Journal of Refrigeration-Revue Internationale Du Froid 31 (3) (2008) 411–422. doi:DOI10.1016/j.ijrefrig.2007.07.013.
URL <GotoISI>://WOS:000254677900008

[7] M. Haida, J. Smolka, M. Palacz, J. Bodys, A. J. Nowak, Z. Bulinski, A. Fic, A. Hafner, K. Banasiak, A. Hafner, Numerical investigation of an r744 liquid ejector for supermarket refrigeration systems, Thermal Science 20 (4) (2016) 1259–1269.
URL http://stacks.iop.org/1742-6596/745/i=3/a=032159

[8] S. Elbel, P. Hrnjak, Flash gas bypass for improving the performance of transcritical r744 systems that use microchannel evaporators, International Journal of Refrigeration-Revue Internationale Du Froid 27 (7) (2004) 724–735. doi:DOI10.1016/j.ijrefrig.2004.07.019.
URL <GotoISI>://WOS:000224937600005

[9] K. Sumeru, H. Nasution, F. N. Ani, A review on two-phase ejector as an expansion device in vapor compression refrigeration cycle, Renewable and Sustainable Energy Reviews 16 (7) (2012) 4927–4937. doi:DOI10.1016/j.rser.2012.04.058.
URL <GotoISI>://WOS:000307909800054

[10] A. Hafner, S. Forsterling, K. Banasiak, Multi-ejector concept for r-744 supermarket refrigeration, International Journal of Refrigeration-Revue Internationale Du Froid 43 (2014) 1–13. doi:DOI10.1016/j.ijrefrig.2013.10.015.
URL <GotoISI>://WOS:000340979900002

[11] P. Gullo, A. Hafner, G. Cortella, Multi-ejector r744 booster refrigerating plant and air conditioning system integration – a theoretical evaluation of energy benefits for supermarket applications, International Journal of Refrigeration (2016) –doi:http://dx.doi.org/10.1016/j.ijrefrig.2016.12.009.
URL //www.sciencedirect.com/science/article/pii/S0140700716304212

[12] F. Liu, Y. Li, E. A. Groll, Performance enhancement of co2 air conditioner with a controllable ejector, International Journal of Refrigeration 35 (6) (2012) 1604–1616. doi:http://dx.doi.org/10.1016/j.ijrefrig.2012.05.005.
URL http://www.sciencedirect.com/science/article/pii/S0140700712001193
[13] K. Banasiak, A. Hafner, E. E. Kriezi, K. B. Madsen, M. Birkelund, K. Fredslund, R. Olsson, Development and performance mapping of a multi-ejector expansion work recovery pack for r744 vapour compression units, International Journal of Refrigeration 57 (2015) 265–276. doi:http://dx.doi.org/10.1016/j.ijrefrig.2015.05.016.
URL http://www.sciencedirect.com/science/article/pii/S0140700715001553
[14] M. Haida, K. Banasiak, J. Smolka, A. Hafner, T. M. Eikevik, Experimental analysis of the r744 vapour compression rack equipped with the multi-ejector expansion work recovery module, International Journal of Refrigeration 64 (2016) 93–107. doi:10.1016/j.ijrefrig.2016.01.017.
URL http://www.sciencedirect.com/science/article/pii/S0140700716000232
[15] X. Chen, M. Worall, S. Omer, Y. Su, S. Riffat, Theoretical studies of a hybrid ejector co2 compression cooling system for vehicles and preliminary experimental investigations of an ejector cycle, Applied Energy 102 (2013) 931 – 942, special Issue on Advances in sustainable biofuel production and use - {XIX} International Symposium on Alcohol Fuels - {ISAF}. doi:http://dx.doi.org/10.1016/j.apenergy.2012.09.032.
URL //www.sciencedirect.com/science/article/pii/S0306261912006733
[16] I. Eames, S. Aphornratana, H. Haider, A theoretical and experimental study of a small-scale steam jet refrigerator, International Journal of Refrigeration 18 (6) (1995) 378 – 386. doi:http://dx.doi.org/10.1016/0140-7007(95)98160-M.
URL //www.sciencedirect.com/science/article/pii/014070079598160M
[17] R. V. Padilla, Y. C. S. Too, R. Benito, R. McNaughton, W. Stein, Thermodynamic feasibility of alternative supercritical co2 brayton cycles integrated with an ejector, Applied Energy 169 (2016) 49 – 62. doi:http://dx.doi.org/10.1016/j.apenergy.2016.02.029.
URL //www.sciencedirect.com/science/article/pii/S0306261916301520
[18] A. Kornhauser, The use of an ejector as a refrigerant expander, in: International Refrigeration and Air Conditioning Conference, Purdue University, Purdue ePubs, The address of the publisher, 1990, pp. 1–11, an optional note.
URL http://docs.lib.purdue.edu/iracc/1102
[19] S. Elbel, N. Lawrence, Mathematical modeling and thermodynamic investigation of the use of two-phase ejectors for work recovery and liquid recirculation in refrigeration cycles, International Journal of Refrigeration 58 (2015) 41–52. doi:http://dx.doi.org/10.1016/j.ijrefrig.2015.06.004.
[20] S. Elbel, N. Lawrence, Review of recent developments in advanced ejector technology, International Journal of Refrigeration 62 (2016) 1–18. doi:http://dx.doi.org/10.1016/j.ijrefrig.2015.10.031.
URL http://www.sciencedirect.com/science/article/pii/S0140700715003266
[21] F. Liu, E. A. Groll, Study of ejector efficiencies in refrigeration cycles, Applied Thermal Engineering 52 (2) (2013) 360 – 370. doi:http://dx.doi.org/10.1016/j.applthermaleng.2012.12.001.
URL //www.sciencedirect.com/science/article/pii/S135943111200806X
[22] C. Richter, Proposal of new object-oriented equation-based model libraries for thermodynamic systems, Ph.D. thesis, Braunschweig University of Technology (2008).
[23] A. Danlos, F. Ravelet, O. Coutier-Delgosha, F. Bakir, Cavitation regime detection through proper orthogonal decomposition: Dynamics analysis of the sheet cavity on a grooved convergent–divergent nozzle, International Journal of Heat and Fluid Flow 47 (2014) 9 – 20. doi:http://dx.doi.org/10.1016/j.ijheatfluidflow.2014.02.001.
URL //www.sciencedirect.com/science/article/pii/S0142727X14000198
[24] T. A. Brenner, R. L. Fontenot, P. G. Cizmas, T. J. O'Brien, R. W. Breault, A reduced-order model for heat transfer in multiphase flow and practical aspects of the proper orthogonal decomposition, Computers and Chemical Engineering 43 (2012) 68 – 80. doi:http://dx.doi.org/10.1016/j.compchemeng.2012.04.003.
URL //www.sciencedirect.com/science/article/pii/S0098135412001056
[25] Z. Ostrowski, R. A. Białecki, A. J. Kassab, Solving inverse heat conduction problems using trained pod-rbf network inverse method, Inverse Problems in Science and Engineering 16 (1) (2008) 39–54. arXiv:http://dx.doi.org/10.1080/17415970701198290, doi:10.1080/17415970701198290.
URL http://dx.doi.org/10.1080/17415970701198290
[26] A. H. Fath, Application of radial basis function neural networks in bubble point oil formation volume factor prediction for petroleum systems, Fluid Phase Equilibria 437 (2017) 14 – 22. doi:http://dx.doi.org/10.1016/j.fluid.2017.01.010.
URL //www.sciencedirect.com/science/article/pii/S0378381217300183
[27] G. Roshani, E. Nazemi, M. Roshani, Intelligent recognition of gas-oil-water three-phase flow regime and determination of volume fraction using radial basis function, Flow Measurement and Instrumentation 54 (2017) 39 – 45. doi:http://dx.doi.org/10.1016/j.flowmeasinst.2016.10.001.
URL //www.sciencedirect.com/science/article/pii/S0955598616301820
[28] C. A. Rogers, A. J. Kassab, E. A. Divo, Z. Ostrowski, R. A. Bialecki, An inverse pod-rbf network approach to parameter estimation in mechanics, Inverse Problems in Science and Engineering 20 (5) (2012) 749–767. doi:10.1080/17415977.2012.693080.
URL http://dx.doi.org/10.1080/17415977.2012.693080
[29] G. Węcel, Z. Ostrowski, P. Kozołub, Absorption line black body distribution function evaluated with proper orthogonal decomposition for mixture pf co2 and h20, International Journal of Numerical Methods for Heat and Fluid Flow 24 (4) (2014) 932–948. doi:http://dx.doi.org/10.1108/HFF-04-2013-0142.
[30] J. Smolka, Z. Bulinski, A. Fic, A. J. Nowak, K. Banasiak, A. Hafner, A computational model of a transcritical r744 ejector based on a homogeneous real fluid approach, Applied Mathematical Modelling 37 (3) (2013) 1208–1224. doi:http://dx.doi.org/10.1016/j.apm.2012.03.044.
URL http://www.sciencedirect.com/science/article/pii/S0307904X12002077

[31] E. W. Lemmon, M. L. Huber, M. O. McLinden, Nist standard reference database 23: Reference fluid thermodynamic and transport properties - refprop, National Institute of Standards and Technology, Standard Reference Data Program.

[32] M. Palacz, J. Smolka, A. Fic, Z. Bulinski, A. J. Nowak, K. Banasiak, A. Hafner, Application range of the hem approach for co2 expansion inside two-phase ejectors for supermarket refrigeration systems, International Journal of Refrigerationdoi:http://dx.doi.org/10.1016/j.ijrefrig.2015.07.006.
URL http://www.sciencedirect.com/science/article/pii/S0140700715002030

[33] K. Banasiak, A. Hafner, Mathematical modelling of supersonic two-phase r744 flows through converging–diverging nozzles: The effects of phase transition models, Applied Thermal Engineering 51 (1–2) (2013) 635 – 643. doi:http://dx.doi.org/10.1016/j.applthermaleng.2012.10.005.
URL //www.sciencedirect.com/science/article/pii/S1359431112006618

[34] M. Palacz, J. Smolka, W. Kus, A. Fic, Z. Bulinski, A. J. Nowak, K. Banasiak, A. Hafner, Cfd-based shape optimisation of a co2 two-phase ejector mixing section, Applied Thermal Engineering 95 (2016) 62–69. doi:http://dx.doi.org/10.1016/j.applthermaleng.2015.11.012.
URL http://www.sciencedirect.com/science/article/pii/S1359431115012478

[35] M. Kirby, L. Sirovich, Application of the karhunen-loeve procedure for the characterization of human faces, IEEE Trans. Pattern Anal. Mach. Intell. 12 (1) (1990) 103–108. doi:10.1109/34.41390.
URL http://dx.doi.org/10.1109/34.41390

[36] S. Walton, O. Hassan, K. Morgan, Reduced order modelling for unsteady fluid flow using proper orthogonal decomposition and radial basis functions, Applied Mathematical Modelling 37 (20–21) (2013) 8930 – 8945. doi:http://dx.doi.org/10.1016/j.apm.2013.04.025.
URL //www.sciencedirect.com/science/article/pii/S0307904X13002771

[37] A. Hafner, K. Banasiak, T. Herdlitschka, K. Fredslund, S. Girotto, M. Haida, J. Smolka, R744 ejector system case: Italian supermarket, spiazzo, 2016, pp. 471–478, cited By 0. doi:10.18462/iir.gl.2016.1078.
URL https://www.scopus.com/inward/record.uri?eid=2-s2.0-85017601791&doi=10.18462%2fiir.gl.2016.1078&partnerID=40&md5=5d10648b38d7b1259701e82a6570e0d0

[38] J. Bodys, M. Palacz, M. Haida, J. Smolka, A. J. Nowak, K. Banasiak, A. Hafner, Full-scale multi-ejector module for a carbon dioxide supermarket refrigeration system: Numerical study of performance evaluation, Energy Conversion and Management 138 (2017) 312 – 326. doi:http://dx.doi.org/10.1016/j.enconman.2017.02.007.
URL http://www.sciencedirect.com/science/article/pii/S019689041730105X